

Fig. 4. Elevation of HMGB1 in serum is induced by skin grafting and mobilizes $\text{Lin}^-/\text{PDGFR}\alpha^+$ cells from BM. (A) Schematic illustration of the Boyden chamber approach to assess migration of the $\text{Lin}^-/\text{PDGFR}\alpha^+$ cells to SSB or PBS. The actual and relative migration of these cells to both buffers is shown. (B) Assessment of $\text{Lin}^-/\text{PDGFR}\alpha^+$ cells migration to heparin-bound (H/B) or unbound (H/U) fractions of the SSB. (C) SDS/PAGE of H/B SSB fractions with $\text{Lin}^-/\text{PDGFR}\alpha^+$ cell migration activity. Results of liquid chromatography-tandem mass spectrometry for three major proteins in the gel are noted on the right. (D) Western blot against nucleolin, AT-III, and HMGB1 in the SSB obtained at sequential time periods. The lowest blot shows $\text{Lin}^-/\text{PDGFR}\alpha^+$ cell migration activities in each SSB. (E) $\text{Lin}^-/\text{PDGFR}\alpha^+$ cell migration assay in a Boyden chamber with recombinant HMGB1, AT-III, and nucleolin. (F) HMGB1 levels in mouse sera after full-thickness skin grafting with newborn wild-type mouse skin. Asterisks (*) indicate statistical significance vs. Day 0 ($P < 0.05$, $n = 4$). (G) Flow cytometric analyses of $\text{Lin}^-/\text{PDGFR}\alpha^+/\text{CD44}^+$ cells of peripheral blood mononuclear cells of mice 12 h after systemic administration of HMGB1 (10 μg in 400 μL of PBS) or PBS (400 μL). Asterisk (*) represents statistical significance ($P < 0.01$, $n = 4$). (H) Intravital two-photon imaging of the calvaria BM in $\text{PDGFR}\alpha\text{-H2BEGFP}$ mice 12 h after systemic administration of PBS (400 μL ; Left) or HMGB1 (10 μg in 400 μL of PBS; Right) via the tail vein. Green color, GFP expressed under the promoter of $\text{PDGFR}\alpha$; red color, BM microvasculature visualized by i.v. injection of 70-kDa dextran-conjugated Texas Red. (Scale bar: 50 μm .)

as an inflammatory regulator. Other studies, however, have indicated that HMGB1 may also act as a local chemo-attractant for various hematopoietic and nonhematopoietic cells that can regulate tissue remodeling (31).

The next objective was to determine the time course for release of the proteins from excised skin graft into the buffer (Fig. 4D). Of note, both HMGB1 and AT-III were rapidly released within a few minutes into the SSB fraction that demonstrated strong chemoattractant activity for $\text{Lin}^-/\text{PDGFR}\alpha^+$ BM cells. AT-III secretion continued at similar levels for at least 48 h, whereas HMGB1 release gradually declined after ≈ 8 h—a time course that paralleled the chemoattraction findings. With regard to nucleolin, its presence in the SSB only started 2 h after incubation, possibly reflecting the consequences of necrosis in the excised skin. To evaluate the chemoattractant properties, we expressed mouse HMGB1 in HEK293 cells and compared the in vitro activity of the purified recombinant protein to induce $\text{Lin}^-/\text{PDGFR}\alpha^+$ BM cell migration. Recombinant AT-III and nucleolin were also assessed, but cell migration assays demonstrated that only HMGB1 could induce migration of these particular BM cells (Fig. 4E). We also explored the nature of the receptor on $\text{Lin}^-/\text{PDGFR}\alpha^+$ BM cells relevant to the cell migration and excluded a role for two known receptors that can mediate the extracellular cytokine effects of HMGB1, the receptor for advanced glycation endproduct (RAGE) and toll-like receptor (TLR) 4 (32–34) (see *SI Results and Discussion* and Fig. S11 for details).

Next, we explored the source of HMGB1 in the grafted skin. Immunofluorescent microscopy analysis of HMGB1 protein in the skin graft showed abundant staining in the epidermis and much less in the dermis, reflecting the higher cellularity in the

epidermis (Fig. S12). We then analyzed Col 7-null mouse skin for HMGB1 release and noted that the detached epithelia (blister roofs) released significant amounts of HMGB1 after soaking in PBS (Fig. S13A and B). These observations suggest that the epithelial tissue in the skin graft could be a significant source of HMGB1 in vivo. Further support for damaged epithelium as a source of HMGB1 was demonstrated by finding elevated HMGB1 in freshly generated subepidermal blister fluid of human subjects with RDEB ($n = 3$) (Fig. S13C). We then investigated the systemic effects of HMGB1 after skin injury. We first measured HMGB1 levels in the sera of mice that had received a skin graft of wild-type newborn mouse skin (Fig. 4F). We observed a marked increase in HMGB1 serum levels 3 d after grafting. Of note, however, no increase in serum HMGB1 was noted in mice with full thickness wounds but no skin graft (Fig. S13D), suggesting that the transplanted epithelial tissue is likely to be the source of the elevated HMGB1 in the sera. We also detected ≈ 60 -fold higher levels of HMGB1 in the sera of individuals with RDEB ($n = 3$) compared with similarly aged normal control subjects ($n = 3$) (Fig. S13E). These observations led us to hypothesize that systemic elevation of HMGB1 in the blood might positively induce recruitment of $\text{Lin}^-/\text{PDGFR}\alpha^+$ cells from BM to raise BM-derived keratinocytes (as well as fibroblasts) in the regenerating injured skin, and that this might be one mechanism through which the practice of skin grafting achieves its clinical goals.

To confirm this hypothesis, we systemically administered recombinant HMGB1 at levels similar to that seen in the sera of skin grafted mice to wild-type mice. We observed that this action could mobilize $\text{Lin}^-/\text{PDGFR}\alpha^+$ BM cells into the blood circulation (Fig. 4G). Lower doses of HMGB1 failed to mobilize

these cells (Fig. S14). We noted no local or systemic inflammation or other potentially adverse effects in the mice, despite the high doses of systemic HMGB1 administered (Fig. S15). To further investigate the mechanics of this mobilization by HMGB1 in vivo, we performed intravital two-photon imaging of calvaria BM in living PDGFR α -H2BGFP mice. This experiment showed that HMGB1 could mobilize PDGFR α -positive cells, allowing them to congregate around blood vessels and, thereby, allow egress into the circulation in vivo (Fig. 4H).

To confirm that the mobilized BM-derived PDGFR α ⁺ circulating cells provide the epithelial cells in vivo, we combined FACS-sorted PDGFR α ⁺/GFP⁺ BM cells with wild-type PDGFR α ⁻ BM cells and transplanted these cells to lethally irradiated mice, which then received skin grafts of Col 7-null mouse skin (Fig. 5A). Very few cells were GFP-positive in the peripheral blood mononuclear cell populations of the PDGFR α ⁺/GFP⁺ BM transplanted mice (Fig. 5B). However, those GFP-positive circulating cells that originated from the transplanted PDGFR α ⁺ BM cells had adherent and proliferative capacities in culture (Fig. 5B). Four weeks after the Col 7-null skin engraftment, multiple foci of GFP-positive cells expressing keratin 5 were observed in the epithelia of the engrafted skin (Fig. 5C), suggesting that the BM-derived PDGFR α ⁺ circulating cells contain a population that can differentiate into epithelial cells in the skin graft.

Discussion

This work clearly demonstrates that Lin⁻/PDGFR α ⁺ cells from BM significantly contribute to the regeneration of the epidermis after skin grafting in vivo, and that one biological repair mechanism involves the key cells being mobilized in response to elevated HMGB1 levels in serum, the source of which is the skin graft. The observation that tissue damage can recruit BM stromal cells for tissue repair is well-established (35), but here we have defined a subpopulation of cells that have the capacity to repair skin, including epidermis. The Lin⁻/PDGFR α ⁺ BM cell marker profile is not unique to one particular cell population, and our data suggest that it is shared by ≈ 1 in 450 BM cells. PDGFR α is not expressed by hematopoietic stem cells but by MSCs in bone marrow that can give rise to mesenchymal lineage cells as well as neuroepithelial and neural crest lineage cells (24–26), suggesting that the Lin⁻/PDGFR α ⁺ BM cells contain an MSC fraction (discussed further in *SI Results and Discussion*).

Our study has shown that in situations in which there is significant damage to the epidermis, such as Col 7 deficiency leading to subepidermal blistering, at least some of the Lin⁻/PDGFR α ⁺ cells have the plasticity to become BM-derived epithelial progenitors, to generate and sustain new keratinocytes, and to correct the intrinsic lack of Col 7. Moreover, we have identified HMGB1 as a specific factor involved in Lin⁻/PDGFR α ⁺ BM cell responses. Our data indicate that HMGB1, which is rapidly released from the detached or blistered Col 7-deficient epithelia, can mobilize Lin⁻/PDGFR α ⁺ BM cells into the circulation and accelerate regeneration of the skin by recruiting these cells to raise BM-derived epithelial cells and BM-derived mesenchymal cells in the epidermis and dermis of Col 7-null skin, respectively.

HMGB1 is a highly conserved, abundant, and ubiquitously expressed 30-kDa nonhistone protein with diverse biologic functions (36, 37). With regards to human and murine HMGB1, only 2 of 215 amino acids show species differences (>99% identical) and both reside in the C-terminal region outside of the known receptor- and DNA-binding motifs (38, 39). HMGB1 can act as a mobile and dynamic nucleo-cytoplasmic protein influencing multiple processes in chromatin such as transcription, replication, recombination, and DNA repair (39, 40), but HMGB1 can also be secreted into the extracellular milieu as a signaling molecule when cells are stressed (41). HMGB1 can bind exogenous and endogenous agents such as endotoxin, microbial DNA, and nucleosomes, and induces adaptive and innate immune responses via TLR2/4/9 followed by NF- κ B activation (42, 43), contributing to inflammation, autoimmune dysregulation, and carcinogenesis. However, purified recombinant HMGB1 has little, if any, proinflammatory activity (44). Indeed, free HMGB1, that is unbound to endogenous/exogenous inflammatory factors, is able to suppress inflammatory reactions in noninjured tissues by inhibiting TLR-mediated NF- κ B signaling (33). Biologically, HMGB1 can be regarded as a critical factor for maintaining tissue homeostasis in cleaning damaged/infected tissues (i.e., promoting intralesional inflammation), but also in protecting surrounding noninjured tissues (i.e., suppressing inflammation), and accelerating regeneration of damaged tissues by mobilizing and recruiting specific BM cells, that include epithelial progenitors when there is extensive epithelial injury, such as in Col 7-deficient RDEB skin.

The concept that a particular threshold concentration of HMGB1 in serum is relevant to mobilizing Lin⁻/PDGFR α ⁺ BM cells and targeting them to damaged tissue also offers unique possibilities to augment a variety of other tissue repair mechanisms. It is likely that, in several other situations, systemic administration of HMGB1 to achieve serum levels similar to those observed in RDEB could be used as a therapeutic strategy to recruit stem/progenitor cells to accelerate regeneration of damaged tissue. Precisely which tissues might benefit from HMGB1-induced mobilization of Lin⁻/PDGFR α ⁺ BM cells remains to be determined. What has also not been determined thus far are the dynamics of both the release of the Lin⁻/PDGFR α ⁺ cells from the BM and the events that promote recruitment and migration within the target tissue and the other potential local microenvironment-

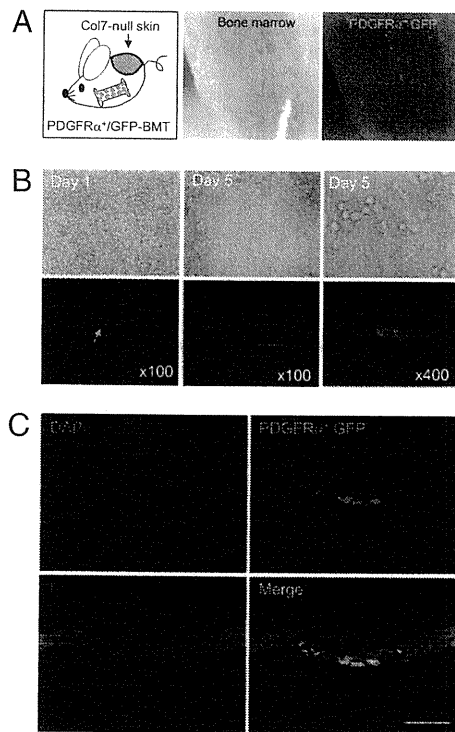


Fig. 5. Mobilized Lin⁻/PDGFR α ⁺ BM-derived cells in circulation contribute to epithelial regeneration of the skin graft in vivo. (A) Schematic illustration showing Col 7-null skin graft on a mouse transplanted with PDGFR α -positive/GFP-BM cells (Left); bright field (Center) and dark field (Right) stereomicroscopic pictures of femoral BM in a PDGFR α ⁺/GFP-BMT mouse. Green fluorescence indicates PDGFR α ⁺/GFP-BM cells. (B) Bright field (Upper) and dark field (Lower) fluorescent microscopic pictures of cultured peripheral blood mononuclear cells that were obtained from the PDGFR α ⁺/GFP-BMT mouse engrafted with Col 7-null skin. (Left) A single PDGFR α ⁺/GFP-BM-derived cell in culture (Day 1). (Center) Proliferation of the single PDGFR α ⁺/GFP-BM-derived cell in culture (Day 5). (Right) Dividing adherent cells indicated in the white lined box in Lower Center. (C) Confocal-laser microscopic pictures of a section of grafted Col7-null skin onto a PDGFR α ⁺/GFP-BMT mouse. GFP fluorescence was merged with the red immunofluorescence of K5 to provide the yellow color. DAPI staining (Upper Left), GFP fluorescence (Upper Right), K5 staining (Lower Left), and a merged image (Lower Right). (Scale bar: 50 μ m.)

induced and biochemical processes that contribute to improved wound healing (35) (discussed further in *SI Materials and Methods*). Nevertheless, we believe our data represent a significant advance in identifying a direction for potentially bringing stem/progenitor cell regenerative medicine to a broader clinical arena.

Materials and Methods

BMT. BM cells were isolated under sterile conditions from 8- to 10-wk-old male C57BL/6 transgenic mice that ubiquitously expressed enhanced green fluorescent protein (GFP). Recipients were 8- to 10-wk-old female C57BL/6 mice that were lethally irradiated with 10 Gy of X-rays, and each irradiated recipient received 5×10^6 BM cells from GFP transgenic mice kindly provided by Masaru Okabe (Osaka University). Experiments were performed on the BMT mice at least 6 wk after the BMT.

Mouse Skin Transplantation. Full-thickness skin from wild-type and Col 7-null newborn mice (graft size $\approx 2 \times 2$ cm) was carefully isolated by excision after the mice had been euthanized under systemic anesthesia, and engrafted onto the backs of the GFP-BMT mice, wild-type BMT mice, and K5-Cre-GFP-BMT mice, with grafting just above the muscular fascia.

- Orkin SH, Zon LI (2008) Hematopoiesis: An evolving paradigm for stem cell biology. *Cell* 132:631–644.
- Prockop DJ (2009) Repair of tissues by adult stem/progenitor cells (MSCs): Controversies, myths, and changing paradigms. *Mol Ther* 17:939–946.
- Fathke C, et al. (2004) Contribution of bone marrow-derived cells to skin: Collagen deposition and wound repair. *Stem Cells* 22:812–822.
- Ishii G, et al. (2005) In vivo characterization of bone marrow-derived fibroblasts recruited into fibrotic lesions. *Stem Cells* 23:699–706.
- Wu Y, Zhao RC, Tredget EE (2010) Concise review: Bone marrow-derived stem/progenitor cells in cutaneous repair and regeneration. *Stem Cells* 28:905–915.
- Krause DS, et al. (2001) Multi-organ, multi-lineage engraftment by a single bone marrow-derived stem cell. *Cell* 105:369–377.
- Hematti P, et al. (2002) Absence of donor-derived keratinocyte stem cells in skin tissues cultured from patients after mobilized peripheral blood hematopoietic stem cell transplantation. *Exp Hematol* 30:943–949.
- Körbling M, et al. (2002) Hepatocytes and epithelial cells of donor origin in recipients of peripheral-blood stem cells. *N Engl J Med* 346:738–746.
- Badiavas EV, Falanga V (2003) Treatment of chronic wounds with bone marrow-derived cells. *Arch Dermatol* 139:510–516.
- Badiavas EV, Abedi M, Butmarc J, Falanga V, Quesenberry P (2003) Participation of bone marrow derived cells in cutaneous wound healing. *J Cell Physiol* 196:245–250.
- Kataoka K, et al. (2003) Participation of adult mouse bone marrow cells in reconstitution of skin. *Am J Pathol* 163:1227–1231.
- Borue X, et al. (2004) Bone marrow-derived cells contribute to epithelial engraftment during wound healing. *Am J Pathol* 165:1767–1772.
- Fan Q, et al. (2006) Bone marrow-derived keratinocytes are not detected in normal skin and only rarely detected in wounded skin in two different murine models. *Exp Hematol* 34:672–679.
- Inokuma D, et al. (2006) CTACK/CCL27 accelerates skin regeneration via accumulation of bone marrow-derived keratinocytes. *Stem Cells* 24:2810–2816.
- Rovó A, Gratwohl A (2008) Plasticity after allogeneic hematopoietic stem cell transplantation. *Biol Chem* 389:825–836.
- Sasaki M, et al. (2008) Mesenchymal stem cells are recruited into wounded skin and contribute to wound repair by transdifferentiation into multiple skin cell type. *J Immunol* 180:2581–2587.
- Fuchs E, Horsley V (2008) More than one way to skin . . . *Genes Dev* 22:976–985.
- Chino T, et al. (2008) Bone marrow cell transfer into fetal circulation can ameliorate genetic skin diseases by providing fibroblasts to the skin and inducing immune tolerance. *Am J Pathol* 173:803–814.
- Tolar J, et al. (2009) Amelioration of epidermolysis bullosa by transfer of wild-type bone marrow cells. *Blood* 113:1167–1174.
- Fujita Y, et al. (2010) Bone marrow transplantation restores epidermal basement membrane protein expression and rescues epidermolysis bullosa model mice. *Proc Natl Acad Sci USA* 107:14345–14350.
- Fine JD, et al. (2008) The classification of inherited epidermolysis bullosa (EB): Report of the Third International Consensus Meeting on Diagnosis and Classification of EB. *J Am Acad Dermatol* 58:931–950.
- Wagner JE, et al. (2010) Bone marrow transplantation for recessive dystrophic epidermolysis bullosa. *N Engl J Med* 363:629–639, and erratum (2010) 363:1383.
- Heinonen S, et al. (1999) Targeted inactivation of the type VII collagen gene (Col7a1) in mice results in severe blistering phenotype: A model for recessive dystrophic epidermolysis bullosa. *J Cell Sci* 112:3641–3648.

Immunofluorescent Microscopy Analysis. The engrafted skins were removed, fixed with 2% paraformaldehyde, and subjected to immunofluorescent analysis. The excised skins were embedded in Tissue-Tec OCT Compound (Sakura Finetek), frozen on dry ice, and stored at -20°C . For immunofluorescence staining, 6- μm -thick sections were labeled with rabbit polyclonal anti-mouse antibodies. Subsequently, sections were stained with goat anti-rabbit IgG secondary antibody.

Cell-Migration Assay. Chemokinetic migration of $\text{Lin}^{-}/\text{PDGFR}\alpha^{+}$ cells was assayed by using a modified Boyden chamber. In brief, 1.0 μg of HMGB1 in 27 μL of DMEM was added in the lower chambers, and 10^6 cells/mL of $\text{Lin}^{-}/\text{PDGFR}\alpha^{+}$ cells suspended in 50 μL of DMEM containing 10% FBS were added to the upper chamber. The cells on the lower side of the membrane were stained with Diff-Quick (Sysmex).

ACKNOWLEDGMENTS. This work was supported by the following grants: a grant from the Northern Osaka (Saito) Biomedical Knowledge-Based Cluster Creation Project; Special Coordination Funds for Promoting Science and a Grant-in-Aid for Scientific Research from the Ministry of Education, Culture, Sports, Science and Technology of Japan; and a Health and Labour Sciences Research Grant (Research of Intractable Diseases) from the Ministry of Health, Labour and Welfare of Japan.

- Takashima Y, et al. (2007) Neuroepithelial cells supply an initial transient wave of MSC differentiation. *Cell* 129:1377–1388.
- Morikawa S, et al. (2009) Prospective identification, isolation, and systemic transplantation of multipotent mesenchymal stem cells in murine bone marrow. *J Exp Med* 206:2483–2496.
- Morikawa S, et al. (2009) Development of mesenchymal stem cells partially originate from the neural crest. *Biochem Biophys Res Commun* 379:1114–1119.
- Bühning HJ, et al. (2009) Phenotypic characterization of distinct human bone marrow-derived MSC subsets. *Ann N Y Acad Sci* 1176:124–134.
- Mongelard F, Bouvet P (2007) Nucleolin: A multifACeTed protein. *Trends Cell Biol* 17: 80–86.
- Quinsey NS, Greedy AL, Bottomley SP, Whisstock JC, Pike RN (2004) Antithrombin: In control of coagulation. *Int J Biochem Cell Biol* 36:386–389.
- Harris HE, Raucci A (2006) Alarmin(g) news about danger: Workshop on innate danger signals and HMGB1. *EMBO Rep* 7:774–778.
- Palumbo R, Bianchi ME (2004) High mobility group box 1 protein, a cue for stem cell recruitment. *Biochem Pharmacol* 68:1165–1170.
- Riuzzi F, Sorci G, Donato R (2006) The amphoterin (HMGB1)/receptor for advanced glycation end products (RAGE) pair modulates myoblast proliferation, apoptosis, adhesiveness, migration, and invasiveness. Functional inactivation of RAGE in L6 myoblasts results in tumor formation in vivo. *J Biol Chem* 281:8242–8253.
- Chen GY, Tang J, Zheng P, Liu Y (2009) CD24 and Siglec-10 selectively repress tissue damage-induced immune responses. *Science* 323:1722–1725.
- Maroso M, et al. (2010) Toll-like receptor 4 and high-mobility group box-1 are involved in iktogenesis and can be targeted to reduce seizures. *Nat Med* 16:413–419.
- Phinney DG, Prockop DJ (2007) Concise review: Mesenchymal stem/multipotent stromal cells: the state of transdifferentiation and modes of tissue repair—current views. *Stem Cells* 25:2896–2902.
- Rauvala H, Rouhiainen A (2010) Physiological and pathophysiological outcomes of the interactions of HMGB1 with cell surface receptors. *Biochim Biophys Acta* 1799: 164–170.
- Sims GP, Rowe DC, Rietdijk ST, Herbst R, Coyle AJ (2010) HMGB1 and RAGE in inflammation and cancer. *Annu Rev Immunol* 28:367–388.
- Baxevas AD, Landsman D (1995) The HMG-1 box protein family: Classification and functional relationships. *Nucleic Acids Res* 23:1604–1613.
- Stros M (2010) HMGB proteins: Interactions with DNA and chromatin. *Biochim Biophys Acta* 1799:101–113.
- Liu Y, Prasad R, Wilson SH (2010) HMGB1: Roles in base excision repair and related function. *Biochim Biophys Acta* 1799:119–130.
- Wang H, et al. (1999) HMG-1 as a late mediator of endotoxin lethality in mice. *Science* 285:248–251.
- Campana L, Bosurgi L, Bianchi ME, Manfredi AA, Rovere-Querini P (2009) Requirement of HMGB1 for stromal cell-derived factor-1/CXCL12-dependent migration of macrophages and dendritic cells. *J Leukoc Biol* 86:609–615.
- Yanai H, et al. (2009) HMGB proteins function as universal sentinels for nucleic-acid-mediated innate immune responses. *Nature* 462:99–103.
- Kazama H, et al. (2008) Induction of immunological tolerance by apoptotic cells requires caspase-dependent oxidation of high-mobility group box-1 protein. *Immunity* 29:21–32.

S1P-targeted therapy for elderly rheumatoid arthritis patients with osteoporosis

Junichi Kikuta · Kaori Iwai · Yukihiro Saeki · Masaru Ishii

Received: 26 April 2010 / Accepted: 14 November 2010 / Published online: 28 November 2010
© Springer-Verlag 2010

Abstract Therapeutics targeting sphingosine-1-phosphate (S1P), a kind of lipid mediator regulating immune cell trafficking, has been emerging rapidly as a novel line of regimen for autoimmune diseases, including rheumatoid arthritis (RA). Here, we propose that S1P-targeted therapy is beneficial not only for limiting inflammation but for preventing bone-resorptive disorders, such as osteoporosis, by controlling the migratory behavior of osteoclast precursors and therefore would be good for treating elderly female RA patients who suffer from postmenopausal osteoporosis and arthritis simultaneously.

Keywords Rheumatoid arthritis · Osteoporosis · Sphingosine-1-phosphate

The emergence of biological agents has undoubtedly caused a paradigm shift in the treatment of rheumatoid arthritis (RA). We rheumatologists are now ambitiously aiming at a 'cure', and not just the 'care', of RA patients and have succeeded in many cases [1]. Despite the brilliant victory over this intractable disease, there are still a large number of underprivileged patients who cannot share in these advances. Elderly RA patients are the main group; many of them cannot receive biological agents due to the high frequency of occurrence of life-threatening infections. Instead, they

are treated with less efficacious disease-modifying anti-rheumatic drugs (DMARDs) and corticosteroids. Oral corticosteroids are still commonly used in clinical practice to relieve inflammation, but this can lead to systemic dysfunction because of the progressive joint damage, which is complicated by severe osteoporosis that increases the vulnerability to fractures of the spine and femur. Recent findings provide such patients with a ray of hope.

Sphingosine-1-phosphate (S1P), a lipid mediator enriched in blood, is a critical regulator of the migration and localization of various cell types, including immune cells [2]. Extensive studies have demonstrated that lymphocytes express S1P₁/Edg-1, a cognate receptor for S1P, which is responsible for their recirculation from lymphoid tissues to the systemic circulation [3]. S1P attracted lot of attention from rheumatologists when FTY720 (Fingolimod), a substance isolated from a Chinese herb and long known to have immunomodulating activity, was shown to be an S1P receptor agonist [4]. Although the detailed mechanism remains elusive, FTY720 acts as an S1P receptor agonist when metabolized and is now emerging as a promising novel immunosuppressive drug that presumably acts by limiting effector lymphocyte egress from lymph nodes. FTY720 is currently being tested clinically in autoimmune diseases such as multiple sclerosis [5], and many other S1P-targeted drugs (S1P receptor agonists or S1P lyase inhibitor) are beginning to be evaluated [6].

Recently, we have demonstrated that S1P was also important for controlling the migration of osteoclasts and their precursors [7]. Using an elaborate intravital two-photon microscopy imaging technique, the migratory behavior of osteoclast precursors in live bone tissues was shown to be critically regulated by S1P, and the intravenous application of an S1P receptor agonist rapidly promoted their exit from bone into blood [8]. It was also

J. Kikuta · K. Iwai · Y. Saeki · M. Ishii
Department of Rheumatology and Clinical Research,
National Osaka-Minami Medical Center, Osaka, Japan

J. Kikuta · M. Ishii (✉)
Laboratory of Biological Imaging,
WPI-Immunology Frontier Research Center, Osaka University,
3-1 Yamada-oka, Osaka, Suita 565-0871, Japan
e-mail: mishii@ifrec.osaka-u.ac.jp

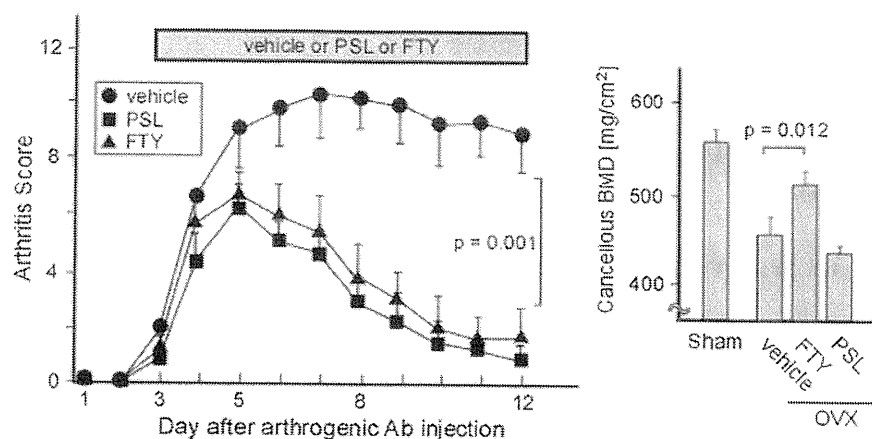


Fig. 1 The therapeutic effects of prednisolone (PSL) and FTY720 (FTY) in mice with both arthritis and osteoporosis. First, 8-week-old ovariectomized mice were injected with 5 mg of an arthrogenic anti-collagen II antibodies cocktail (Chondrex, Redmond, WA) at day 0, and then with 50 μ g of lipopolysaccharide (LPS) (0111:B4, Sigma-Aldrich, St. Louis, MO) 3 days later (9). Prednisolone (PSL, 0.5 mg/

kg/day), FTY720 (1 mg/kg/day), or vehicle only was administered every day beginning on day 3. The arthritis scores are shown in the left panel. The error bars represent the SEM ($n = 5$ per group). The cancellous bone mineral density (BMD) of the femur was analyzed by pQCT (LCT-200, Aloka, Japan) after killing the mice at day 14. Error bars represent the SEM ($n = 5$ per group)

demonstrated that treatment with the S1P receptor agonist FTY720 relieved ovariectomy-induced osteoporosis in mice (a model of postmenopausal osteoporosis in women), by facilitating osteoclast recirculation into blood and reducing the number of mature osteoclasts attached to the bone surface, which suggests a new line of therapy against bone-resorptive disorders [7]. These studies suggest that S1P-targeted therapy would be particularly beneficial for treating RA patients with both immunological and bone-resorptive disorders.

Inspired by this concept, we further examined the therapeutic effect of the S1P receptor agonist FTY720 on simultaneous disease involving both arthritis and osteoporosis (Fig. 1). Ovariectomized mice were injected with an arthrogenic anti-collagen II antibodies cocktail and then with lipopolysaccharide (LPS), so that they developed arthritis in their paws [9]. These mice exhibit both arthritis and osteoporosis and can be regarded as a model of elderly female RA patients. To treat the arthritis, prednisolone (PSL, 0.5 mg/kg/day), FTY720 (1 mg/kg/day), or vehicle only, was administered every day beginning on day 3, and the arthritis score was calculated [10]. We also evaluated bone mineral homeostasis by analyzing the cancellous bone mineral density (BMD) of the femur on day 14. The results showed that the S1P receptor agonist FTY720 was as potent as corticosteroid for suppressing arthritis; in addition, FTY720 recovered the ovariectomy-induced bone density loss, whereas prednisolone did not. As expected, these results clearly suggest that S1P-targeted therapy, such as with S1P receptor agonists, would be beneficial for treating elderly female RA patients who suffer from postmenopausal osteoporosis and arthritis simultaneously.

The effect of S1P receptor agonists is very rapid [4], and robust immunosuppressive effects (by sequestering lymphocytes) can be observed within a few hours after oral administration, although they do not last long (usually disappearing within 12–24 h). Therefore, the profile of an S1P receptor agonist would be similar to that of corticosteroid, rather than to those of methotrexate or other DMARDs. A variety of anticipated S1P-targeted drugs might replace corticosteroids for relieving the inflammation of RA and become a part of the standard RA treatment in the near future. This would be especially conducive to improving the quality of life of elderly patients, who have been left behind so far.

References

1. Van Vollenhoven RF (2009) Treatment of rheumatoid arthritis: state of the art 2009. *Nat Rev Rheumatol* 5:531–541
2. Rosen H, Sphingosine Goetzl EJ (2005) 1-phosphate and its receptors: an autocrine and paracrine network. *Nat Rev Immunol* 5:560–570
3. Matloubian M, Lo CG, Cinamon G, Lesneski MJ, Xu Y, Brinkmann V et al (2004) Lymphocyte egress from thymus and peripheral lymphoid organs is dependent on S1P receptor 1. *Nature* 427:355–360
4. Mandala S, Hajdu R, Bergstrom J, Quackenbush E, Xie J, Milligan J et al (2002) Alteration of lymphocyte trafficking by sphingosine-1-phosphate receptor agonists. *Science* 296:346–349
5. Kappos L, Antel J, Comi G, Montalban X, O'Connor P, Polman CH et al (2006) on behalf of the FTY720 D2201 Study Group. Oral fingolimod (FTY720) for relapsing multiple sclerosis. *N Engl J Med* 355:1124–1140
6. Japtok L, Kleuser B (2009) The role of sphingosine-1-phosphate receptor modulators in the prevention of transplant rejection, autoimmune diseases. *Curr Opin Investig Drugs* 10:1183–1194

7. Ishii M, Egen JG, Klauschen F, Meier-Schellersheim M, Saeki Y, Vacher J et al (2009) Sphingosine-1-phosphate mobilizes osteoclast precursors and regulates bone homeostasis. *Nature* 458:524–528
8. Klauschen F, Ishii M, Qi H, Bajénoff M, Egen JG, Germain RN et al (2009) Quantifying cellular interaction dynamics in 3D fluorescence microscopy data. *Nat Protoc* 4:1305–1311
9. Terato K, Hasty KA, Reife RA, Cremer MA, Kang AH, Stuart JM (1992) Induction of arthritis with monoclonal antibodies to collagen. *J Immunol* 148:2103–2108
10. Sasai M, Saeki Y, Ohshima S, Nishioka K, Mima T, Tanaka T et al (1999) Delayed onset and reduced severity of collagen-induced arthritis in interleukin-6-deficient mice. *Arthritis Rheum* 42:1635–1643

In Vivo Fluorescence Imaging of Bone-Resorbing Osteoclasts


Toshiyuki Kowada,[†] Junichi Kikuta,^{‡,§} Atsuko Kubo,^{‡,§} Masaru Ishii,^{‡,§} Hiroki Maeda,[¶] Shin Mizukami,^{†,¶} and Kazuya Kikuchi^{‡,¶,¶}

[†]Laboratory of Chemical Imaging Techniques, Immunology Frontier Research Center (IFReC), Osaka University, Osaka, Japan

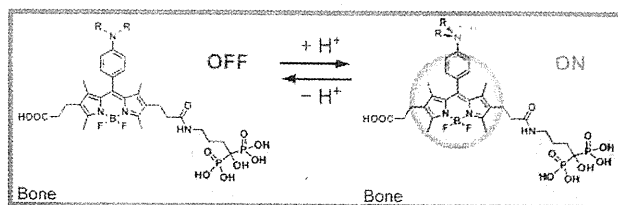
[‡]Laboratory of Cellular Dynamics, Immunology Frontier Research Center (IFReC), Osaka University, Osaka, Japan

[§]Japan Science and Technology Agency (JST), CREST, Tokyo, Japan

[¶]Department of Material and Life Science, Graduate School of Engineering, Osaka University, Osaka, Japan

 Supporting Information

ABSTRACT: Osteoclasts are giant polykaryons responsible for bone resorption. Because an enhancement or loss of osteoclast function leads to bone diseases such as osteoporosis and osteopetrosis, real-time imaging of osteoclast activity in vivo can be of great help for the evaluation of drugs. Herein, pH-activatable chemical probes BAp-M and BAp-E have been developed for the detection of bone-resorbing osteoclasts in vivo. Their acid dissociation constants (pK_a) were determined as 4.5 and 6.2 by fluorometry in various pH solutions. These pK_a values should be appropriate to perform selective imaging of bone-resorbing osteoclasts, because synthesized probes cannot fluoresce intrinsically at physiological pH and the pH in the resorption pit is lowered to about 4.5. Furthermore, BAp-M and BAp-E have a bisphosphonate moiety that enabled the probes to localize on bone tissues. The hydroxyapatite (HA) binding assay in vitro was, therefore, performed to confirm the tight binding of the probes to the bone tissues. Our probes showed intense fluorescence at low pH values but no fluorescence signal under physiological pH conditions on HA. Finally, we applied the probes to in vivo imaging of osteoclasts by using intravital two-photon microscopy. As expected, the fluorescence signals of the probes were locally observed between the osteoclasts and bone tissues, that is, in resorption pits. These results indicate that our pH-activatable probes will prove to be a powerful tool for the selective detection of bone-resorbing osteoclasts in vivo, because this is the first instance where in vivo imaging has been conducted in a low-pH region created by bone-resorbing osteoclasts.



INTRODUCTION

Osteoclasts are giant multinucleated cells derived from monocytoic hematopoietic cells, which are responsible for bone resorption within the bone-remodeling compartment.^{1–4} Because an enhancement or loss of osteoclast function causes bone diseases such as osteoporosis or osteopetrosis, real-time imaging of osteoclast activity in vivo is one of the most important tools required for investigations of osteoclast functions.⁴ However, current bone imaging techniques such as computed tomography (CT) and biochemical markers of bone metabolism cannot connect spatial information with cellular activity. To overcome this problem, fluorescence imaging is a promising technique for obtaining temporal and spatial information about target cells or proteins.⁵ Thus, we sought to develop fluorescent chemical probes with an OFF/ON switch, which can selectively detect active osteoclasts and thereby instantaneously provide an image of the location of the osteoclasts activated by particular stimuli. Furthermore, two-photon excitation microscopy can provide noninvasive imaging of osteoclasts in vivo.⁶

Active osteoclasts resorb the organic and inorganic components of the bone tissues by cathepsin K secretion and by proton extrusion, which causes acidification of the bone surface.⁴ To the

best of our knowledge, there have been no reports on the detection of protons extruded by osteoclasts. Only a single report has demonstrated the indirect in vivo detection of cathepsin K activity.⁷ However, the cathepsin K probe has not yet provided real-time imaging data about the osteoclasts in the process of resorbing bone tissues, and its selectivity as a probe for the detection of osteoclast formation is inadequate.

We recognized that active osteoclasts can be selectively detected through specific imaging of low-pH regions by using a pH-activatable fluorescent probe⁸ with specific delivery of the probe using a bisphosphonate group⁹ (Figure 1a). In addition, this probe should be quite useful in the evaluation of drugs.

There are two requirements for the development of new probes for selective detection of bone-resorbing osteoclasts. One obvious requirement is a pH-sensitive fluorescence switch, and the other is the capability to localize on the bone tissue. Therefore, we designed fluorescent probes called “BAps”. These probes are composed of boron–dipyromethene (BODIPY) dye and a bisphosphonate group (Figure 1b). BODIPY dyes are

Received: July 12, 2011

Published: September 22, 2011

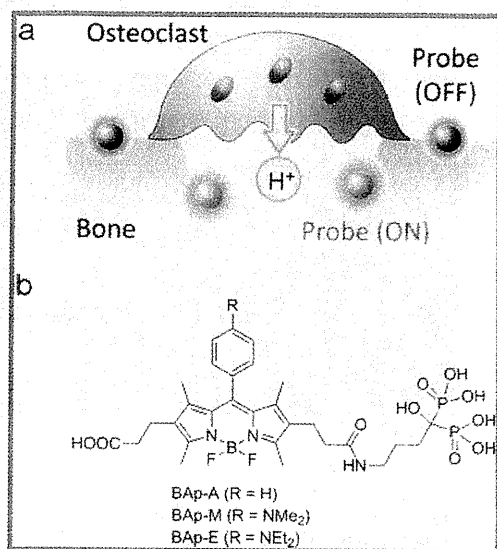


Figure 1. Strategy for selective detection of bone-resorbing osteoclasts using pH-activatable probes and design of BAPs. (a) pH-activatable probes are immobilized on the bone tissue and provide intense fluorescence only when osteoclasts are resorbing bone. (b) Structures of the pH-activatable probes (BAPs).

well-known fluorophores that have been used in a large number of applications because of their environmental stability, large molar absorption coefficients, and high fluorescence quantum yields.¹⁰ Most recently, pH-activatable fluorescence probes including a BODIPY dye have been developed for the detection of cancers and real-time monitoring of therapy.¹¹ Furthermore, bisphosphonate compounds are currently used as drugs for the treatment of various bone diseases. These compounds chelate calcium and inhibit bone resorption. We, therefore, decided to combine a BODIPY-based pH-sensing unit with a bisphosphonate compound.

RESULTS AND DISCUSSION

Characterization of BAPs. To demineralize the bone matrix, osteoclasts secrete protons (H^+) into the resorption pit where the pH value is lowered to about 4.5.³ We, therefore, considered that selective imaging of osteoclasts would be achieved by the development of pH-activatable probes with an acid dissociation constant (pK_a) in the range of 4.5–6.5, because those probes cannot intrinsically fluoresce at the physiological pH. According to this assumption, we designed and synthesized three fluorescent probes with different pK_a values (Figure 1b). A control probe with “always-ON” fluorescence (BAP-A) was developed. The other probes are fluorescence “turn-ON” type sensors that can detect the acidic pH environment. Since the fluorescence OFF/ON switching mechanism is based on photoinduced electron transfer (PeT), the pK_a values of these probes can be finely tuned by the appropriate choice of an electron-donating moiety attached to the BODIPY core.¹² Thus, we chose *p*-dimethylanilino (BAP-M) and *p*-diethylanilino groups (BAP-E) as the electron-donating moieties to provide pK_a values in the range of 4.5–6.5.

The fluorescent probes were synthesized in one step from the corresponding dicarboxylic acids by using straightforward synthetic pathways (Scheme S1, Supporting Information). To confirm the pH-dependent fluorescence properties of BAPs, we

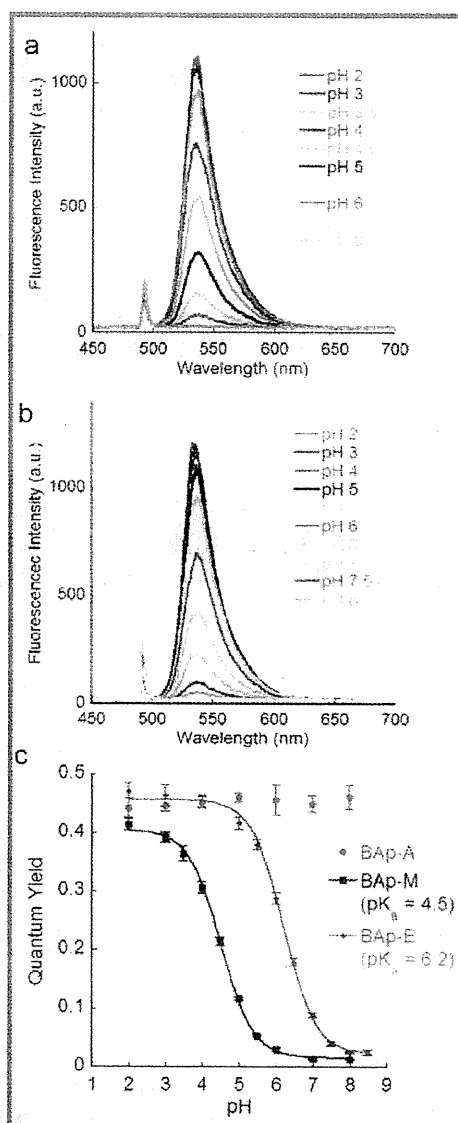


Figure 2. Fluorescence spectra (0.2 μ M, excited at 492 nm) of (a) BAP-M and (b) BAP-E in citrate-phosphate buffer, and (c) pH-dependent profiles of changes in fluorescence quantum yield of BAPs. The data were fitted to the Henderson–Hasselbalch equation.

measured the absorption and emission spectra in citrate-phosphate buffer at different pH values (Figures S1 and 2). All three probes had absorption maxima at about 520 nm. These peaks were found to be independent of the pH of the buffer. These results indicate that any structural changes or aggregations of the dye induced by pH changes do not occur in aqueous solution. In contrast, the fluorescence intensities of BAP-M and BAP-E were highly affected by the pH (Figure 2). The fluorescence intensities of BAP-M and BAP-E decreased along with an increase in pH. Essentially, no fluorescence was observed at the physiological pH. This phenomenon can be rationalized by the observation that PeT actually occurs from the *p*-anilino group to the BODIPY core.¹² Thus, these two probes showed a fluorescence “turn-ON” type increase at lower pH. Furthermore, the pK_a values were estimated by fitting pH-dependent changes of the fluorescence quantum yield to the

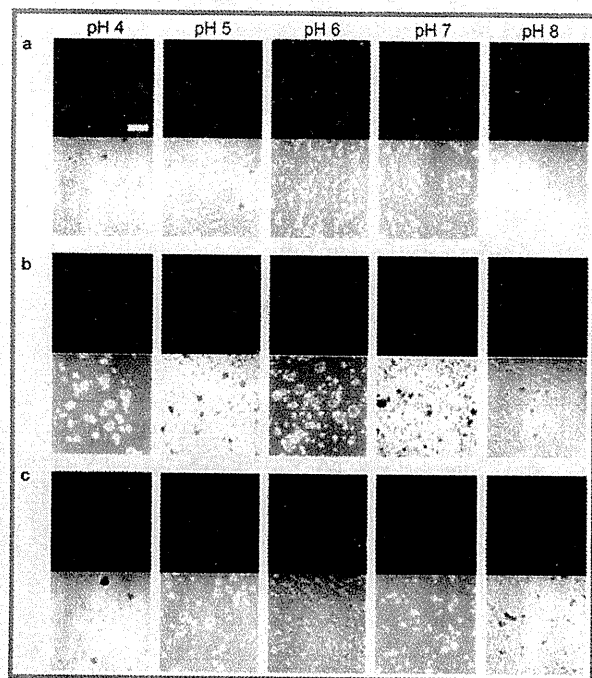


Figure 3. Confocal microscope images of BAp binding to hydroxyapatite in McIlvaine's citrate-phosphate buffer. Scale bar: 40 μm . (a) BAp-A. (b) BAp-M. (c) BAp-E.

Henderson–Hasselbalch equation (Figure 2c). Consequently, the $\text{p}K_a$ values of BAp-M and BAp-E were 4.5 and 6.2, respectively. These results indicate that the two pH-activatable probes could be used to selectively visualize the bone-resorbing osteoclasts. On the other hand, BAp-A showed intense fluorescence regardless of pH changes as would be expected by an “always-ON” fluorescence probe.

Hydroxyapatite Binding Test. Bone tissues are mainly composed of type I collagen and hydroxyapatite (HA). Confocal microscopy was then performed to ascertain the HA binding activity and the fluorescence properties of BAp bound to HA. Intense fluorescence was observed from every HA particle, which was mixed with BAp-A and soaked in buffer at different pH values (Figure 3). We next examined the pH-activatable probes, namely, BAp-M and BAp-E. In the case of BAp-M, the fluorescence signals from HA particles were hardly observed under physiological conditions, i.e., at pH 7.0 and pH 8.0. The fluorescence intensities gradually increased with the decrease in the pH value, and consequently, intense fluorescence was observed below pH 5.0. Similar to the behavior in solution, the HA particle including BAp-E responded in an environment of higher pH relative to BAp-M, and showed intense fluorescence. However, the fluorescence signals were very weak or not observed at pH 7.0 or 8.0. These results indicate that BAp is pH-sensitive not only in aqueous solution but also in the solid state, when bound to HA. It was thus expected that synthesized probes could be immobilized on bone tissue and that they will retain their pH-sensitive properties in vivo.

In Vivo Imaging of Osteoclasts. To clarify the osteoclast function and develop new therapeutic agents to treat bone diseases, real-time monitoring of living osteoclasts in vivo will be very important. However, it is challenging to observe living osteoclasts that are present in the medullary cavity, deep inside the bone.

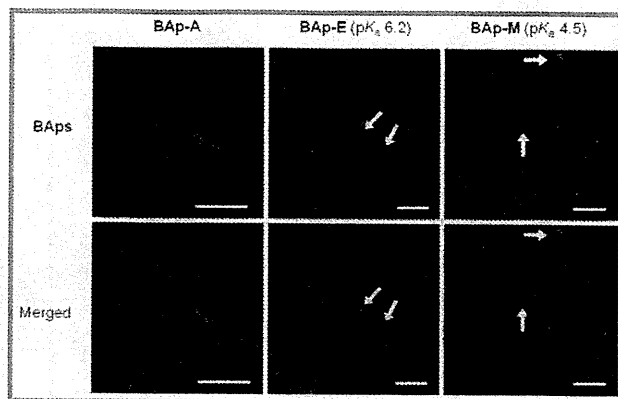


Figure 4. Two-photon excitation microscopy images of in vivo osteoclasts using BAp. PBS solution of BAp (green) was subcutaneously administered daily for 3 days to TRAP-tdTomato (red) transgenic mice. Second harmonic generation from collagen in the bone matrix is presented as a blue signal. Scale bars: 40 μm .

We used two-photon excitation microscopy, which can penetrate deeply into tissues, to capture images of osteoclasts through the parietal bone of mice.⁶ The parietal bone is relatively thin, and the distance between the bone surface and the medullary cavity is 80–120 μm . This allowed us to achieve real-time imaging of the active osteoclasts in vivo. To ensure that BAp can function in a living mouse, we administered the probes to mice and evaluated their pH-sensitive properties by the above-described method (Figure 4). The blue signal indicates second harmonic generation from collagen fibers in the bone matrix. It is obvious that osteoclasts were present in the medullary cavity, because we used TRAP (tartrate-resistant acid phosphatase)-tdTomato transgenic mice, in which TRAP-positive mature osteoclasts predominantly express tdTomato.¹³ To confirm whether the synthesized probes can be transported and immobilized on the bone tissues, we first used the “always-ON” probe BAp-A (Figure 4). As expected, green fluorescence was observed all over the bone surface. We next examined in vivo imaging of osteoclasts by using pH-activatable probes. In contrast to the case of BAp-A, green signals were locally observed only between the osteoclasts and the bone tissues (Figure 4, white arrow). Although the green staining was also observed in the lower left of the BAp-E panels, it is mainly derived from second harmonic generation from the bone matrix (Figure S2, Supporting Information). These results indicate that our probes are functioning properly, and have the potential to detect the bone-resorbing osteoclasts in vivo. Moreover, it is expected that the pH value in the resorption pit created by an osteoclast should be within the range of 4–6, because more intense fluorescence is found using BAp-E, which has a higher $\text{p}K_a$ value relative to BAp-M. The brightness of BAp-E ($\epsilon_{\text{abs},450} \times \Phi$) between pH 4 and pH 6 is roughly 1.2–7.5 times as intense as that of BAp-M. Until now, the pH value in the resorption pit had not been measured in vivo. Therefore, we expect that this method will be helpful to estimate the pH value in the resorption pits.

CONCLUSION

We demonstrated that our custom-designed probes, in particular, BAp-E, fluoresce in the low-pH environment created by osteoclasts in vivo, as well as in a cuvette. From medicinal and

therapeutic points of view, an imaging technique for visualizing the migration and function of osteoclasts is highly desirable. Because this method is the first example of *in vivo* imaging of a low-pH region created by bone-resorbing osteoclasts, we are confident that the pH-activatable probes BAPs will provide a powerful tool for the selective detection of bone-resorbing osteoclasts *in vivo*.

EXPERIMENTAL SECTION

Synthesis of BAP-A. To a solution of the corresponding bis-carboxylic acid (1,3,5,7-tetramethyl-2,6-bis(2-carboxyethyl)-8-phenyl-4,4-difluoro-4-bora-3a,4a-diaza-s-indacene)¹¹ (9.40 mg, 20.1 μ mol) in MeCN (5 mL) were added alendronic acid (5.00 mg, 20.1 μ mol) in water (4 mL), 2 N aq NaOH (60 μ L, 120 μ mol), and DMT-MM (27.7 mg, 100 μ mol) at room temperature. After being stirred for 16 h, the reaction mixture was poured into 10% aqueous solution of AcOH (11 mL) and lyophilized. The crude compound was then purified by reverse-phase HPLC under the following conditions: A/B = 85/15 (0 min) to 10/90 (30 min) (solvent A: 100 mM aq TEAA; solvent B: acetonitrile). Compound eluted with a retention time of 12 min was collected. After lyophilization, an orange powder of BAP-A·3Et₃N was obtained (6.55 mg, 6.53 μ mol) in 32% yield. ¹H NMR (400 MHz, D₂O) δ 0.95 (s, 3H), 0.97 (s, 3H), 1.12 (t, *J* = 7.2 Hz, 27H), 1.64–1.67 (m, 2H), 1.75–1.85 (m, 2H), 2.01–2.09 (m, 4H), 2.25–2.37 (m, 10H), 3.00–3.07 (m, 20H), 6.71 (br s, 2H), 7.14 (br s, 3H). HRMS (FAB[−]) Calcd for [M − H⁺][−] 698.2021, found 698.2010.

Synthesis of BAP-M. BAP-M was synthesized from the corresponding bis-carboxylic acid (1,3,5,7-tetramethyl-2,6-bis(2-carboxyethyl)-8-(*p*-dimethylaminophenyl)-4,4-difluoro-4-bora-3a,4a-diaza-s-indacene)¹¹ by the same method as described above and purified by reverse-phase HPLC under the following conditions: A/B = 75/25 (0 min) to 60/40 (20 min), and then 10/90 (25 min) (solvent A: 100 mM aq TEAA; solvent B: acetonitrile). An orange powder of BAP-M·3Et₃N (*t*_R = 11 min) was obtained in 9% yield. ¹H NMR (400 MHz, D₂O) δ 1.10–1.14 (m, 33H), 1.63 (br s, 2H), 1.78 (br s, 2H), 2.02–2.10 (m, 4H), 2.28 (s, 3H), 2.32 (s, 3H), 2.41 (br s, 4H), 2.74 (s, 6H), 2.97–3.06 (m, 20H), 6.71 (br s, 4H). HRMS (FAB[−]) Calcd for [M − H⁺][−] 741.2443, found 741.2462.

Synthesis of BAP-E. BAP-E was synthesized from the corresponding bis-carboxylic acid (1,3,5,7-tetramethyl-2,6-bis(2-carboxyethyl)-8-(*p*-diethylaminophenyl)-4,4-difluoro-4-bora-3a,4a-diaza-s-indacene)¹¹ by the same method as described above and purified by reverse-phase HPLC under the following conditions: A/B = 80/20 (0 min) to 10/90 (30 min) (solvent A: 100 mM aq TEAA; solvent B: acetonitrile). An orange powder of BAP-E·3Et₃N (*t*_R = 13 min) was obtained in 11% yield. ¹H NMR (400 MHz, D₂O) δ 0.95 (t, *J* = 7.2 Hz, 6H), 1.08 (s, 3H), 1.13 (t, *J* = 7.2 Hz, 27H), 1.18 (s, 3H), 1.60–1.65 (m, 2H), 1.71–1.83 (m, 2H), 2.03–2.11 (m, 4H), 2.28 (s, 3H), 2.35 (s, 3H), 2.40–2.46 (m, 4H), 2.93–2.98 (m, 2H), 3.05 (q, *J* = 7.2 Hz, 18H), 3.34 (q, *J* = 7.2 Hz, 4H), 6.93 (d, *J* = 8.0 Hz, 2H), 7.07 (d, *J* = 8.4 Hz, 2H). HRMS (FAB[−]) Calcd for [M − H⁺][−] 769.2756, found 769.2743.

High-Performance Liquid Chromatography. We performed HPLC on a system composed of a pump (PU-2080, JASCO) and a detector (MD-2010, JASCO) with an Inertsil ODS-3 (4.6 mm \times 250 mm for analysis; 10.0 mm \times 250 mm for preparation).

Fluorometry. Fluorescence spectra were measured in McIlvaine's citrate-phosphate buffer using a Hitachi F4500 spectrometer. Slit width was 2.5 nm for both excitation and emission, and the photomultiplier voltage was 950 V. Fluorescence quantum yields were determined using fluorescein in 0.1 N NaOH as a standard (Φ = 0.85, λ_{ex} = 492 nm).

In Vitro Hydroxyapatite Binding Test. Five milligrams/mL of hydroxyapatite was vortexed in a 1 μ M aqueous solution of BAPs (1 mL) for 30 min at room temperature. The mixture was centrifuged and

washed four times with water. A portion of the residual powder was soaked in citrate-phosphate buffer (400 μ L) at various pH values in a glass-bottom dish. Fluorescence images were then collected using a confocal laser scanning microscope (Olympus, FLUOVIEW FV10i) equipped with a 60 \times lens. The excitation wavelength was 473 nm, and the emission was filtered with a BA490–590 filter.

Two-Photon Excitation Imaging in Mice. The generation of TRAP promoter-tdTomato transgenic mice has been described elsewhere.¹³ Twenty-five micrograms/body of BAP-A, BAP-E, or BAP-M dissolved in PBS was injected subcutaneously into TRAP-tdTomato mice once a day beginning 3 days prior to the recording of images. Intravital microscopy of mouse calvaria bone tissues was performed using a protocol modified from a previous study.⁶ Mice were anesthetized with isoflurane (Escaïn; 2% vaporized in 100% oxygen), and the hair at the neck and scalp was removed with hair removal lotion (Kracie). The frontoparietal skull was exposed, and the mouse head was immobilized in a custom-designed stereotactic holder. The imaging system was composed of a multiphoton microscope (SP5; Leica) driven by a laser (Mai-Tai HP Ti: Sapphire; Spectraphysics) tuned to 900 nm and an upright microscope (DM6000B; Leica) equipped with a 20 \times water immersion objective (HCX APO, N.A. 1.0; Leica). The microscope was enclosed in an environmental chamber in which anesthetized mice were warmed by heated air. Fluorescent probes were detected through a bandpass emission filter at 525/50 nm. Osteoclasts were visualized by expression of TRAP-tdTomato (detected using a 585/40 nm filter). Snapshot images were acquired, and raw imaging data were processed with Imaris (Bitplane) with a Gaussian filter for noise reduction. *In vivo* imaging experiments were performed three times for each probe, and representative images are shown.

ASSOCIATED CONTENT

S Supporting Information. Synthetic scheme, photophysical properties, and high-performance liquid chromatograms of BAPs, and images of negative control experiment *in vivo*. This material is available free of charge via the Internet at <http://pubs.acs.org>.

AUTHOR INFORMATION

Corresponding Author

kkikuchi@mls.eng.osaka-u.ac.jp

ACKNOWLEDGMENT

This work was partially supported by the Japan Society for the Promotion of Science (JSPS) through its "Funding Program for World-Leading Innovative R&D on Science and Technology (FIRST) Program" and by the Ministry of Education, Culture, Sports, Science and Technology (MEXT) of Japan (Grant No. 22108519 and 20675004). K.K. and M.I. express their special thanks for support from the Takeda Science Foundation and the Mochida Memorial Foundation. K.K. also thanks the Naito Foundation for financial support. K.K. and S.M. acknowledge the Asahi Glass Foundation for financial support.

REFERENCES

- (1) Boyle, W. J.; Simonet, W. S.; Lacey, D. L. *Nature* **2003**, *423*, 337–342.
- (2) Raggatt, L. J.; Partridge, N. C. *J. Biol. Chem.* **2010**, *285*, 25103–25108.
- (3) Teitelbaum, S. L. *Science* **2000**, *289*, 1504–1508.
- (4) Rodan, G. A.; Martin, T. J. *Science* **2000**, *289*, 1508–1514.

- (5) (a) Marks, K. M.; Nolan, G. P. *Nat. Methods* **2006**, *3*, 591–596. (b) Hinner, M. J.; Johnsson, K. *Curr. Opin. Biotechnol.* **2010**, *21*, 766–776. (c) Giepmans, B. N. G.; Adams, S. R.; Ellisman, M. H.; Tsien, R. Y. *Science* **2006**, *312*, 217–224. (d) Sadhu, K. K.; Mizukami, S.; Hori, Y.; Kikuchi, K. *ChemBioChem* **2011**, *12*, 1299–1308.
- (6) Ishii, M.; Egen, J. G.; Klauschen, F.; Meier-Schellersheim, M.; Saeki, Y.; Vacher, J.; Proia, R. L.; Germain, R. N. *Nature* **2009**, *458*, 524–528.
- (7) Kozloff, K. M.; Quinti, L.; Patntirapong, S.; Hauschka, P. V.; Tung, C.-H.; Weissleder, R.; Mahmoodet, U. *Bone* **2009**, *44*, 190–198.
- (8) (a) Han, J.; Burgess, K. *Chem. Rev.* **2010**, *110*, 2709–2728. (b) Wang, R.; Yu, C.; Yu, F.; Chen, L. *Trends Anal. Chem.* **2010**, *29*, 1004–1013.
- (9) (a) Roelofs, A. J.; Coxon, F. P.; Ebetino, F. H.; Lundy, M. W.; Henneman, Z. J.; Nancollas, G. H.; Sun, S.; Blazewska, K. M.; Bala, J. L. F.; Kashemirov, B. A.; Khalid, A. B.; McKenna, C. E.; Rogers, M. J. *J. Bone Miner. Res.* **2010**, *25*, 606–616. (b) Kashemirov, B. A.; Bala, J. L. F.; Chen, X.; Ebetino, F. H.; Xia, Z.; Russell, R. G. G.; Coxon, F. P.; Roelofs, A. J.; Rogers, M. J.; McKenna, C. E. *Bioconjugate Chem.* **2008**, *19*, 2308–2310. (c) Zaheer, A.; Lenkinski, R. E.; Mahmood, A.; Jones, A. G.; Cantley, L. C.; Frangioni, J. V. *Nat. Biotechnol.* **2001**, *19*, 1148–1154.
- (10) (a) Loudet, A.; Burgess, K. *Chem. Rev.* **2007**, *107*, 4891–4932. (b) Ulrich, G.; Ziessel, R.; Harriman, A. *Angew. Chem., Int. Ed.* **2008**, *47*, 1184–1201.
- (11) Urano, Y.; Asanuma, D.; Hama, Y.; Koyama, Y.; Barrett, T.; Kamiya, M.; Nagano, T.; Watanabe, T.; Hasegawa, A.; Choyke, P. L.; Kobayashi, H. *Nat. Med.* **2009**, *15*, 104–109.
- (12) (a) Sunahara, H.; Urano, Y.; Kojima, K.; Nagano, T. *J. Am. Chem. Soc.* **2007**, *129*, 5597–5604. (b) Gabe, Y.; Urano, Y.; Kikuchi, K.; Kojima, H.; Nagano, T. *J. Am. Chem. Soc.* **2004**, *126*, 3357–3367.
- (13) Kikuta, J.; Wada, Y.; Kowada, T.; Wang, Z.; Sun-Wada, G.-H.; Shimazu, Y.; Nishiyama, I.; Kubo, A.; Mizukami, S.; Maiya, N.; Yasuda, H.; Kikuchi, K.; Germain, R. N.; Ishii, M. Unpublished.

The sphingosine-1-phosphate transporter Spns2 expressed on endothelial cells regulates lymphocyte trafficking in mice

Shigetomo Fukuhara,¹ Szandor Simmons,^{2,3} Shunsuke Kawamura,^{2,3} Asuka Inoue,⁴ Yasuko Orba,⁵ Takeshi Tokudome,⁶ Yuji Sunden,⁷ Yuji Arai,⁸ Kazumasa Moriwaki,⁹ Junji Ishida,¹⁰ Akiyoshi Uemura,⁹ Hiroshi Kiyonari,¹¹ Takaya Abe,¹¹ Akiyoshi Fukamizu,¹⁰ Masanori Hirashima,⁹ Hirofumi Sawa,⁵ Junken Aoki,⁴ Masaru Ishii,^{2,3} and Naoki Mochizuki¹

¹Department of Cell Biology, National Cerebral and Cardiovascular Center Research Institute, Osaka, Japan. ²Laboratory of Cellular Dynamics, World Premier International Research Center—Immunology Frontier Research Center, Osaka University, Osaka, Japan. ³Japan Science and Technology, Core Research for Evolutional Science and Technology (CREST), Tokyo, Japan. ⁴Laboratory of Molecular and Cellular Biochemistry, Graduate School of Pharmaceutical Sciences, Tohoku University, Miyagi, Japan. ⁵Department of Molecular Pathobiology, Hokkaido University Research Center for Zoonosis Control, Sapporo, Japan. ⁶Department of Biochemistry, National Cerebral and Cardiovascular Center Research Institute, Osaka, Japan. ⁷Laboratory of Comparative Pathology, Hokkaido University School of Veterinary Medicine, Sapporo, Japan. ⁸Department of Molecular Biology, National Cerebral and Cardiovascular Center Research Institute, Osaka, Japan. ⁹Division of Vascular Biology, Department of Physiology and Cell Biology, Kobe University Graduate School of Medicine, Hyogo, Japan. ¹⁰Life Science Center, Tsukuba Advanced Research Alliance, University of Tsukuba, Ibaraki, Japan, and Graduate School of Life and Environmental Sciences, University of Tsukuba, Ibaraki, Japan. ¹¹Laboratory for Animal Resources and Genetic Engineering, RIKEN Center for Developmental Biology, Hyogo, Japan.

The bioactive lysophospholipid mediator sphingosine-1-phosphate (S1P) promotes the egress of newly formed T cells from the thymus and the release of immature B cells from the bone marrow. It has remained unclear, however, where and how S1P is released. Here, we show that in mice, the S1P transporter spinster homolog 2 (Spns2) is responsible for the egress of mature T cells and immature B cells from the thymus and bone marrow, respectively. Global *Spns2*-KO mice exhibited marked accumulation of mature T cells in thymi and decreased numbers of peripheral T cells in blood and secondary lymphoid organs. Mature recirculating B cells were reduced in frequency in the bone marrow as well as in blood and secondary lymphoid organs. Bone marrow reconstitution studies revealed that *Spns2* was not involved in S1P release from blood cells and suggested a role for *Spns2* in other cells. Consistent with these data, endothelia-specific deletion of *Spns2* resulted in defects of lymphocyte egress similar to those observed in the global *Spns2*-KO mice. These data suggest that *Spns2* functions in ECs to establish the S1P gradient required for T and B cells to egress from their respective primary lymphoid organs. Furthermore, *Spns2* could be a therapeutic target for a broad array of inflammatory and autoimmune diseases.

Introduction

Sphingosine-1-phosphate (S1P) is a bioactive lysophospholipid mediator that plays a crucial role in diverse physiological functions, such as lymphocyte trafficking, vascular development, and inflammation (1–5). S1P exerts biological functions mostly through activating cell-surface G protein-coupled receptors S1P1–S1P5, while intracellular S1P is also known to act as a second messenger to regulate inflammation (6). It remains unclear how intracellular S1P is transported to the outside of the cells to activate S1P receptors expressed on the cells.

The activation of S1P1 signaling in lymphocytes by S1P has been shown to promote the egress of newly formed T cells from the thymus and that of mature T and B cells from secondary lymphoid organs such as spleen and lymph nodes (7–10). An immunosuppressive molecule, FTY720, produces peripheral lymphopenia by blocking the lymphocyte egress from the thymus and lymph nodes. Interestingly, FTY720 was found to elicit the immunosuppressive effect by functionally antagonizing the S1P/S1P1 signaling pathway (8, 11–13). In fact, this compound has been recently approved by the United States Food and Drug Administration for treatment of autoimmune diseases (14). In addition, S1P/S1P1

receptor signals direct the release of immature B cells from the bone marrow to the peripheral blood (15, 16).

The concentration of S1P is abundant in circulatory fluids, such as blood and lymph (~ μ M), whereas it is normally kept low in the lymphoid tissues (~nM) by S1P-degrading enzymes that include lipid phosphate phosphatase 3 (17, 18). However, it has been suggested that this concentration difference of S1P is required but not sufficient for lymphocyte egress from lymphoid tissues into the circulation (9), implying the significance of S1P gradient made in lymphoid tissues. Consistently, S1P produced by neural crest-derived perivascular cells is required for efficient T cell egress (19). Moreover, lymphatic ECs release S1P, which is necessary for lymphocyte egress from lymph nodes into lymph (20). However, it is still unclear how B and T cell egress from the primary lymphoid organs and which cells release S1P that promotes the egress of these cells.

S1P is generated inside of the cell by phosphorylation of sphingosine in a reaction catalyzed by sphingosine kinase 1 and 2, closely related isozymes, and is exported toward the outside of the cell to stimulate its cell-surface receptors (21, 22). Release of S1P is observed in a variety of cells, such as platelets, erythrocytes, mononuclear cells, neutrophils, mast cells, and ECs (3, 21–28). In vitro analyses have revealed that ABC transporters mediate S1P release in several types of cells, such as mast cells, erythrocytes, platelets, breast cancer cells, and

Conflict of interest: The authors have declared that no conflict of interest exists.

Citation for this article: *J Clin Invest.* 2012;122(4):1416–1426. doi:10.1172/JCI60746.

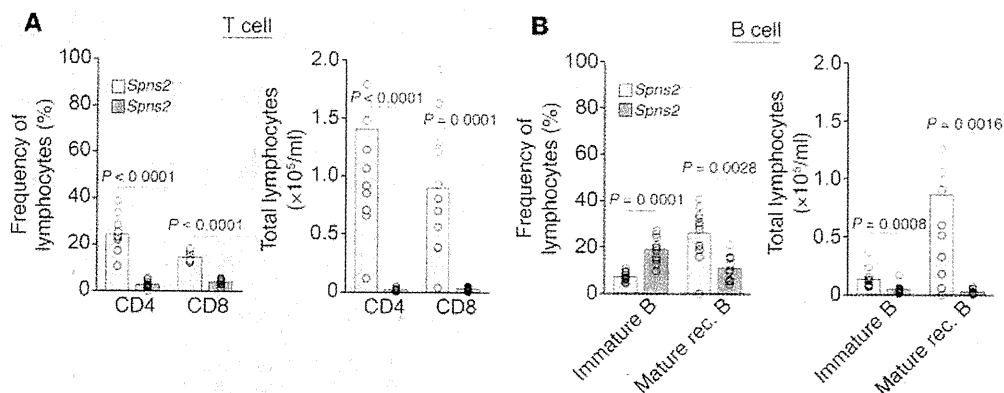


Figure 1

Mature T and recirculating mature B lymphocytes are remarkably reduced in the peripheral blood of *Spns2*^{-/-} mice. (**A** and **B**) Flow cytometric analyses of control (*Spns2*^{+/+}) and global *Spns2*^{-/-} mice. (**A**) Frequencies (left) and total numbers (right) of CD4 SP (CD4) and CD8 SP (CD8) T cells in peripheral blood are shown ($n = 11$). (**B**) Frequencies (left) and total numbers (right) of immature B cells (CD19⁺CD23-IgD-IgM⁺, immature B) and mature recirculating B cells (CD19⁺CD23⁺IgD⁺, Mature rec. B) in peripheral blood are shown ($n = 11$). In **A** and **B**, bars and circles indicate averages and values for individual mice, respectively.

astrocytes (24, 29–32). We and others have identified the S1P transporter spinster homolog 2 (*Spns2*) as an S1P transporter in zebra fish (33, 34). However, the physiological functions of *Spns2* in mammals remain totally unknown. Furthermore, S1P transporters responsible for S1P-mediated lymphocyte trafficking have not been identified.

In the present study, we investigated the importance of *Spns2* in lymphocyte trafficking by analyzing the *Spns2*-deficient mice and found that *Spns2* is responsible for egress of mature T cells and immature B cells from thymus and bone marrow, respectively. We further revealed, by performing bone marrow reconstitution studies and by analyzing mice with conditional deletion of *Spns2* in ECs, that ECs release S1P through *Spns2*, thereby promoting lymphocyte egress from both thymus and bone marrow.

Results

Spns2 is essential for trafficking of both T and B cells. To address the physiological functions of *Spns2* in mammals, we generated global *Spns2*-KO (*Spns2*^{-/-}) mice by crossing *Spns2*^{fl/fl} mice, in which exon 2 of the *Spns2* gene is flanked with loxP sites, with mice expressing Cre recombinase under the control of cytomegalovirus promoter (Supplemental Figure 1; supplemental material available online with this article; doi:10.1172/JCI160746DS1). RT-PCR analyses of the RNA extracted from the lungs of WT and *Spns2*^{-/-} mice revealed that *Spns2*^{-/-} mice express a mutant mRNA transcript lacking exon 2-derived sequence encoding aa 124–145 of WT *Spns2* (Supplemental Figure 2, A and B). This *Spns2* mutant protein failed to localize at the plasma membrane and lost the ability to export S1P (Supplemental Figure 2, C and D). Thus, we conclude that *Spns2*^{-/-} mice are indeed functionally disrupted for *Spns2*.

Spns2^{-/-} mice develop normally, survive to adulthood, and are fertile, although they exhibited symblepharon to a greater or lesser extent (Supplemental Figure 3). In addition, blood biochemical examination revealed no significant differences between WT and *Spns2*^{-/-} mice (Supplemental Figure 4). Notably, hematological analysis showed a significant decrease in white blood cell count in *Spns2*^{-/-} mice compared with control mice, although there were no differences in the other hematological parameters, such as red blood cells, platelets, hemoglobin, hematocrit, mean corpuscular

volume, mean corpuscular hemoglobin, and mean corpuscular hemoglobin concentration (Supplemental Figure 5), implying the role of *Spns2* in lymphocyte trafficking.

It should be noted that the number and proportion of mature CD4 and CD8 single-positive (SP) T cells was dramatically reduced in the blood of *Spns2*^{-/-} mice (Figure 1A and Supplemental Figure 6A). In addition, immature B cells (CD19⁺CD23-IgD-IgM⁺) and mature recirculating B cells (CD19⁺CD23⁺IgD⁺) were decreased in the blood of *Spns2*^{-/-} mice compared with WT mice (Figure 1B and Supplemental Figure 6B). These findings suggest that *Spns2* is involved in trafficking of both T and B lymphocytes.

Spns2 regulates T cell egress from the thymus into blood. To study the cause of the decrease in mature T lymphocytes in the blood of *Spns2*^{-/-} mice, we examined the thymus where T lymphocytes develop and from which they egress into blood. *Spns2*^{-/-} mice exhibited normal thymus structures (Supplemental Figure 7). The numbers and proportions of mature CD4 and CD8 SP T cells in the thymi of *Spns2*^{-/-} mice were increased compared with those of WT mice, although there was no significant change in the number of immature CD4/CD8 double-positive (DP) T cells and CD4/CD8 double-negative (DN) progenitor thymocytes (Figure 2, A and B). These data suggest a significant role for *Spns2* in modulating the egress of mature T cells from the thymus into the blood.

During final maturation of CD4 and CD8 SP T cells in the medulla of the thymus, they downregulate CD69, upregulate S1P1 and CD62L, and consequently migrate out of the thymus in response to S1P (35–38). Thus, we examined the semi-mature (CD69^{lo}CD62L^{lo}) and fully mature (CD69^{lo}CD62L⁺) SP T cells in the thymi of *Spns2*^{-/-} mice. The proportion of fully mature SP T cells was increased in comparison with that of WT mice, while the relative amount of semi-mature SP T cells was decreased (Supplemental Figure 8, A and B). In addition, the cell-surface expression of CD69 on the fully mature SP T cells was slightly higher in *Spns2*^{-/-} mice than in WT mice (Supplemental Figure 8C). Since S1P is suggested to be required for full CD69 downregulation during final maturation of SP thymocytes (8, 36, 39), this may be due to a decreased release of S1P in thymus of *Spns2*^{-/-} mice. These results indicate that *Spns2* is involved in the release of S1P required for T cell egress from the thymus into the blood.

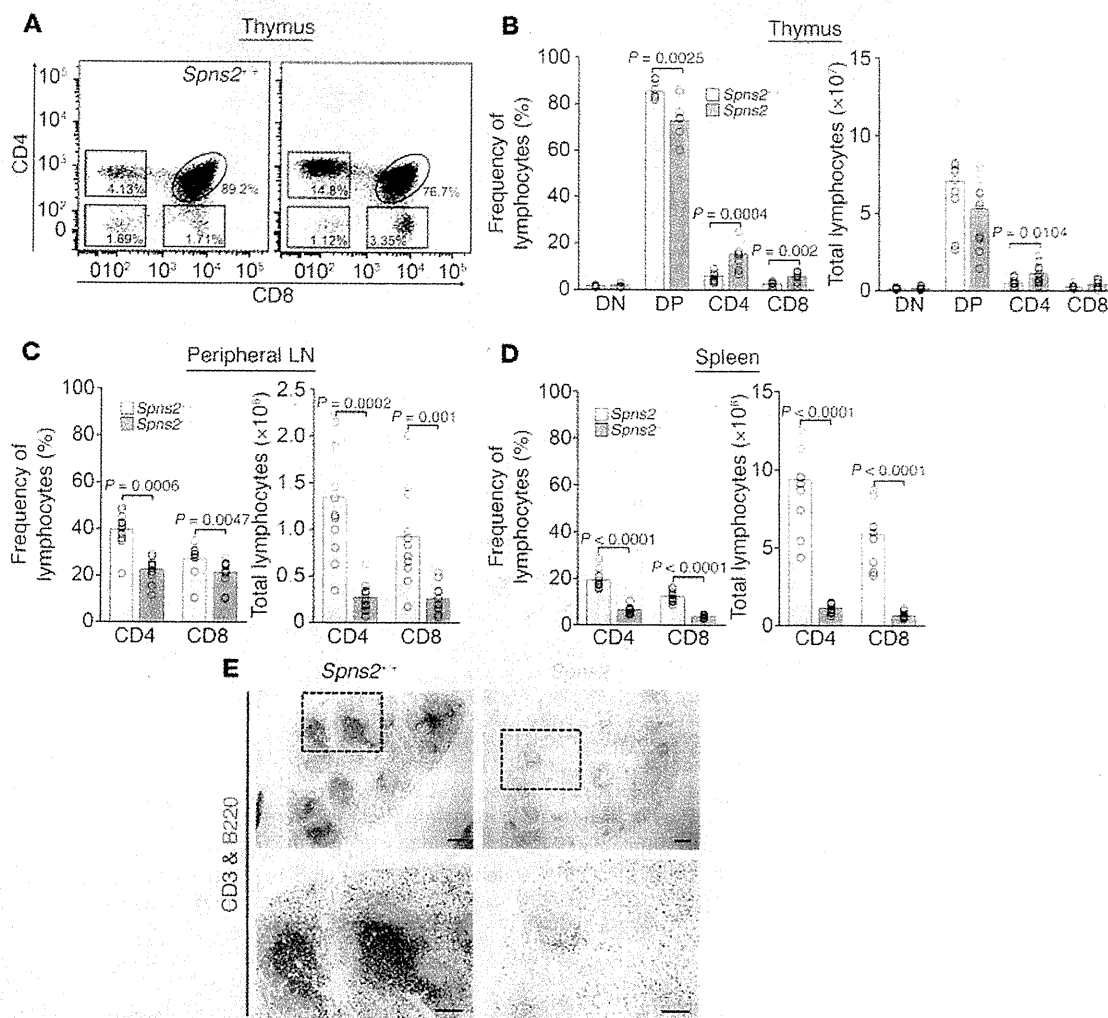


Figure 2

Egress of mature T cells from the thymus is impaired in *Spns2*^{-/-} mice. (A–D) Flow cytometric analyses of control (*Spns2*^{+/+}) and global *Spns2*^{-/-} mice. (A) A representative flow cytometric analysis of T cells in the thymus. The numbers represent the percentages of CD4 SP, CD8 SP, CD4/CD8 DP T cells, and CD4/CD8 DN thymocytes. (B) Frequencies (left) and total numbers (right) of CD4/CD8 DN (DN), CD4/CD8 DP (DP), CD4 SP (CD4) and CD8 SP (CD8) thymocytes and T cells are shown ($n = 11$). (C) Frequencies and numbers of CD4 SP (CD4) and CD8 SP (CD8) T cells in peripheral lymph nodes are shown ($n = 11$). (D) Frequencies and numbers of CD4 SP (CD4) and CD8 SP (CD8) T cells in spleens are shown ($n = 11$). In B–D, bars and circles indicate averages and values for individual mice, respectively. (E) Spleen sections from control (*Spns2*^{+/+}) or *Spns2*^{-/-} mice, stained to detect CD3⁺ T cells (blue) and B220⁺ B cells (red). The boxed areas of upper panels are enlarged in lower panels. Scale bars: 200 μ m (top row); 50 μ m (bottom row).

To assess the possibility that lack of mature T cells in the blood of *Spns2*^{-/-} mice is related to their accumulation in other secondary lymphoid tissues, we further examined mature SP T lymphocytes in peripheral lymph nodes and in the spleen. In contrast with the accumulation of mature T cells in the thymus, the numbers and proportions of mature CD4 and CD8 SP T cells were dramatically reduced in peripheral lymph nodes and in the spleen of *Spns2*^{-/-} mice, although their structures were normal (Figure 2, C–E, and Supplemental Figure 7). These results show that a decrease in the number of mature T cells in the peripheral blood of *Spns2*^{-/-} mice is a consequence of impaired T cell egress from the thymus, but not due to the accumulation in the secondary lymphoid organs.

Spns2 regulates egress of immature B cells from the bone marrow into the blood. In the late stage of B cell development in the bone marrow, newly

generated immature B cells are exported into the peripheral blood in an S1P/S1P1 signal-dependent manner (15, 16). The immature B cells subsequently undergo maturation in the secondary lymphoid tissues and migrate back to the bone marrow through the blood (recirculating mature B cells). To explore the cause of remarkable reduction of recirculating mature B lymphocytes in the peripheral blood of *Spns2*^{-/-} mice, we examined the number and proportion of the lymphocytes at different developmental stages. The numbers and frequencies of mature recirculating B cells (B220^{hi}IgM⁺ or CD19⁺IgM⁺IgD⁻) were significantly reduced in the bone marrow of *Spns2*^{-/-} mice compared with that of control mice (Figure 3, A and B, and Supplemental Figure 9). However, the number of pro-/pre-B cells (B220^{lo}IgM⁻) and immature B cells (B220^{lo}IgM⁺ or CD19⁺IgM⁺IgD⁻) was normal in the bone marrow of *Spns2*^{-/-} mice, although their frequencies were slightly

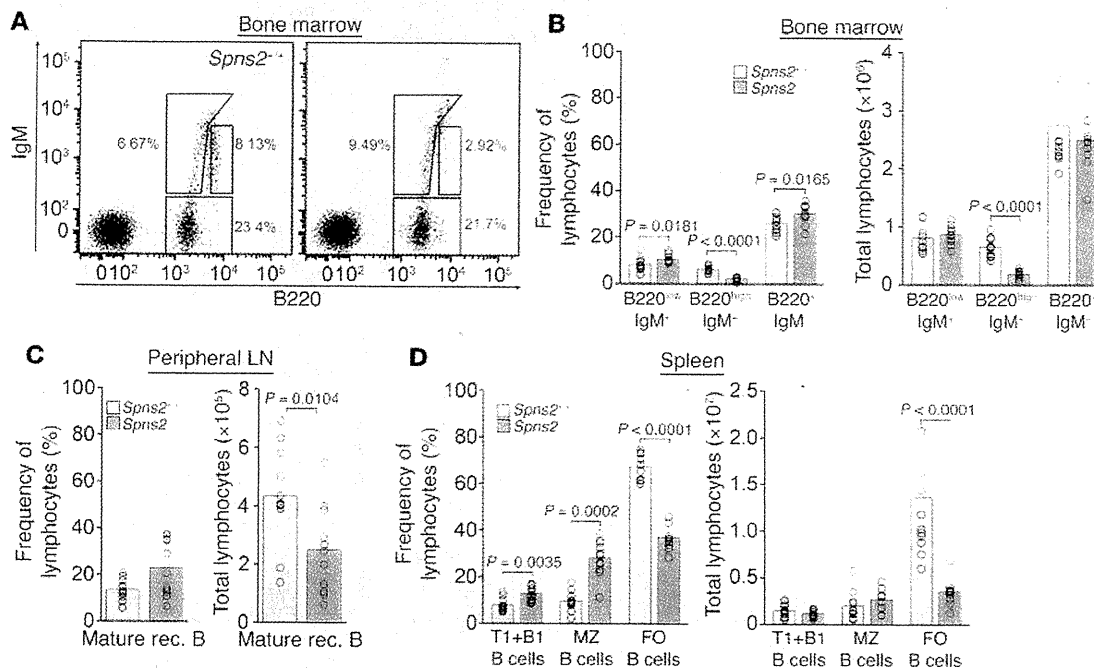


Figure 3 Immature B cell egress from bone marrow is impaired in *Spns2*^{-/-} mice. (A–D) Flow cytometric analysis of B cells in control (*Spns2*^{+/+}) and *Spns2*^{-/-} mice. (A) A representative flow cytometric analysis of progenitor B (B220⁺IgM⁻), immature B (B220^{lo}IgM⁺) and mature recirculating B cells (B220^{hi}IgM⁺) in the bone marrow cavity. Numbers indicate the percentages of IgM⁻ and B220-expressing cells of total lymphocytes. (B) Frequencies (left) and total numbers of pro-/pre-B cells (B220⁺IgM⁻), immature B cells (B220^{lo}IgM⁺), and mature recirculating B cells (B220^{hi}IgM⁺) defined as in A are shown (n = 11). (C) Frequencies (left) and numbers (right) of mature recirculating B (mature rec. B) cells (CD19⁺CD23⁺IgD⁺) in peripheral lymph nodes are shown (n = 11). (D) Frequencies (left) and numbers (right) of T1 B cells (CD19⁺CD21⁻CD23⁻), MZ (CD19⁺CD21⁺CD23^{lo}), and follicular B cells (FO) (CD19⁺CD21^{lo}CD23⁺) in spleens are shown (n = 11). In B–D, bars and circles indicate averages and values for individual mice, respectively.

higher than those in control mice, probably due to the reduction of mature recirculating B cell count (Figure 3, A and B, and Supplemental Figure 9). Together with the evidence for the decreased number of immature B cells in the peripheral blood of *Spns2*^{-/-} mice (Figure 1B), these results suggest that the egress of immature B cells from the bone marrow is impaired in *Spns2*^{-/-} mice.

To further confirm this conclusion, we examined the number and proportion of B lymphocytes in the secondary lymphoid organs. In the peripheral lymph nodes, the number of mature B cells was reduced in *Spns2*^{-/-} mice, although the frequency of mature B cells was not different from that in control mice (Figure 3C). In the spleen, the numbers and proportions of follicular B cells were significantly decreased in *Spns2*^{-/-} mice compared with those of control mice, although there was no difference in the number of marginal zone (MZ) and transitional type 1 (T1) and B1 B cells between control and *Spns2*^{-/-} mice (Figure 3D). These results reveal that the decrease in mature recirculating B cells in the peripheral blood of *Spns2*^{-/-} mice is not due to their accumulation in the secondary lymphoid organs, although it remains unclear whether *Spns2* is involved in the egress of B lymphocytes from the secondary lymphoid organs. Therefore, we conclude that *Spns2* is required for the egress of immature B cells from the bone marrow into the blood.

Spns2 is not involved in S1P release from blood cells. Which cells expressing *Spns2* are responsible for releasing S1P necessary for lymphocyte trafficking? Blood cells, especially erythrocytes, are known to produce S1P, thereby contributing to high plasma S1P concentration

(9, 23–26). Thus, we first investigated whether *Spns2* is involved in S1P release from blood cells. In *Spns2*^{-/-} mice, plasma S1P levels were reduced to 54% of those in control mice (0.39 ± 0.03 μM in control mice; 0.21 ± 0.01 μM in *Spns2*^{-/-} mice), although plasma sphingosine and glycerolosphospholipids of *Spns2*^{-/-} mice were comparable to those in control mice (Figure 4, A–H). Most of the plasma S1P is known to be associated with HDL and albumin (40–42). Consistent with the reduced concentration of plasma S1P in *Spns2*^{-/-} mice, the amount of S1P associated with HDL and albumin was lower in *Spns2*^{-/-} mice than in WT mice (Supplemental Figure 10).

To further clarify whether the reduction of plasma S1P concentration in *Spns2*^{-/-} mice is attributed to the decreased S1P release from blood cells, we examined the secretion of S1P from blood cells isolated from either control or *Spns2*^{-/-} mice. S1P release from blood cells occurred in *Spns2*^{-/-} mice to an extent similar to that in control mice (Figure 5A). This S1P release was not caused by membrane damage, since no release was observed when the cells were incubated at 4°C (Figure 5A), as previously reported (27). These results suggest that *Spns2* is not involved in the release of S1P from blood cells. To further confirm this conclusion, we performed bone marrow reconstitution studies (Supplemental Figure 11). Reconstitution of irradiated *Spns2*^{-/-} mice with WT bone marrow did not restore the reduced concentration of plasma S1P (Figure 5B). Furthermore, *Spns2*^{-/-} mice reconstituted with WT bone marrow still exhibited accumulation of mature SP T lymphocytes in the thymus and reduction of mature recirculating B cells in the bone marrow in comparison with WT mice (Figure 5,

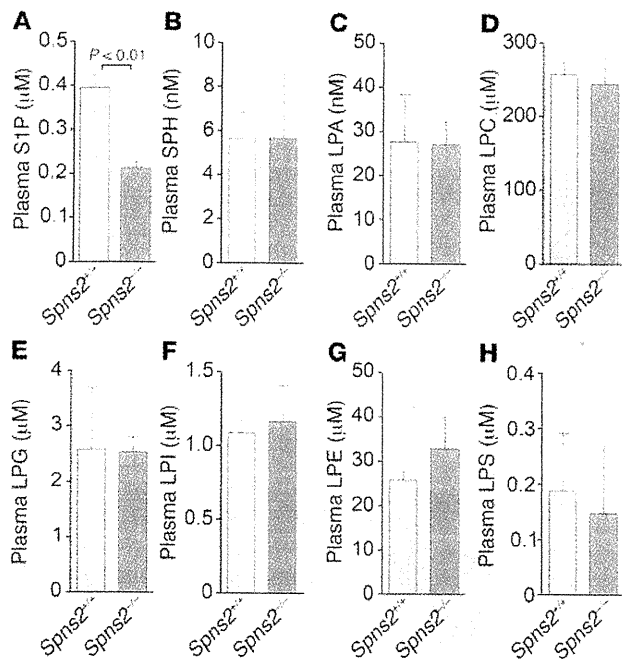


Figure 4 Plasma S1P concentration is reduced in *Spns2*^{-/-} mice. (A–H) Plasma concentrations of S1P (A), sphingosine (SPH) (B), LPA (C), LPC (D), LPG (E), LPI (F), LPE (G), and LPS (H) in control (*Spns2*^{+/+}) or *Spns2*^{-/-} mice. Data are shown as mean ± SD (*n* = 3–5).

C and D). These findings indicate that cells other than blood cells expressing *Spns2* secrete S1P to control lymphocyte trafficking.

Spns2 mediates S1P release from ECs. Cultured vascular ECs produce S1P in vitro (43, 44), although S1P release from vascular ECs has not been confirmed in vivo. Another type of EC, lymphatic ECs, secrete S1P into lymph, thereby regulating lymphocyte egress from lymph nodes (20). Thus, we next investigated whether *Spns2* is involved in the release of S1P from ECs. RT-PCR analyses revealed that *Spns2* is expressed not only in lymphatic ECs, but also in several types of vascular ECs (Figure 6A). In addition, depletion of *Spns2* by siRNA resulted in the inhibition of S1P release from ECs (Figure 6, B and C). Furthermore, we investigated whether *Spns2* is expressed in ECs in vivo by performing in situ hybridization analyses. *Spns2* mRNA was clearly expressed on the ECs in the thymus (Figure 6D). Although it has been reported that pericytes covering thymic ECs release S1P to promote T cell egress from thymus (19), we could not detect expression of *Spns2* mRNA on the pericytes in the thymus (Figure 6D). Besides the thymus, expression of *Spns2* mRNA was also observed in the ECs of other tissues, such as heart, lung, and hypothalamus, but not in those of kidney and olfactory bulb (Supplemental Figure 12). These results suggest that ECs secrete S1P through *Spns2*. Hence, we hypothesized that S1P released from ECs via *Spns2* is required for lymphocyte egress from primary lymphoid organs.

ECs regulate thymic egress by releasing S1P through Spns2. To address whether *Spns2* functions in ECs to regulate lymphocyte trafficking, we tried to generate mice lacking *Spns2* in ECs (*Spns2*-ECKO: *Spns2*^{fl/fl}; *Tie2Cre*) by crossing the *Spns2*^{fl/fl} mice with the mice expressing Cre recombinase under the *Tie2* promoter (Supplemental Figure 1). In *Spns2*-ECKO mice, plasma S1P concentration was decreased to the level observed in *Spns2*^{-/-} mice (Supplemental Fig-

ure 13), indicating that ECs release S1P into plasma in an *Spns2*-dependent manner. *Spns2*-ECKO mice develop normally without symblepharon formation that is observed in global *Spns2*^{-/-} mice, suggesting that *Spns2* acts as an S1P transporter not only in ECs but also in other types of cells.

We further investigated whether *Spns2* functions in ECs to promote T cell egress from the thymus by S1P. Compared with control mice, the proportion of mature CD4 and CD8 SP T cells was increased in the thymus of *Spns2*-ECKO mice, but to a lesser extent than that in *Spns2*^{-/-} mice (Figure 2A and Figure 7A). In addition, the number and proportion of CD4 and CD8 SP T cells in *Spns2*-ECKO mice were dramatically decreased in the peripheral blood, spleen, and peripheral lymph nodes (Figure 7, B and C, and Supplemental Figure 14), suggesting an impaired thymic egress of mature T lymphocytes in *Spns2*-ECKO mice into the peripheral lymphoid organs. The *Tie2* promoter is active not only in ECs, but also in hematopoietic cells (45–47). To further confirm that the phenotype of *Spns2*-ECKO mice is attributed to the impaired function of *Spns2* in ECs, we performed bone marrow reconstitution experiments. *Spns2*-ECKO mice reconstituted with control bone marrow exhibited accumulation of mature CD4 and CD8 SP T cells in the thymus, and their deficiency in the peripheral blood compared with control mice reconstituted with control bone marrow (Supplemental Figure 15). These findings apparently reveal that S1P released from ECs through *Spns2* is involved in the egress of mature T cells from the thymus into the blood.

ECs promote the egress of immature B cells from the bone marrow by releasing S1P through Spns2. We further investigated the role of ECs in immature B cell egress from the bone marrow. As observed in *Spns2*^{-/-} mice, the numbers and proportions of mature recirculating B cells, but not pro-/pre-B cells and immature B cells, were remarkably decreased in the bone marrow of *Spns2*-ECKO mice in comparison with control mice (Figure 8A and Supplemental Figure 16). Mature recirculating B cells in the blood and peripheral lymph nodes of *Spns2*-ECKO mice were decreased (Figure 8B and Supplemental Figure 17). Furthermore, the numbers and frequencies of follicular B cells were significantly reduced in the spleen of *Spns2*-ECKO mice compared with control mice (Figure 8C), although the number of MZ B cells in the spleen was comparable between WT and *Spns2*-ECKO mice. Unexpectedly, the spleens of *Spns2*-ECKO mice have increased numbers of T1 and B1 B cells compared with those of control mice. This result may imply a more complex role of *Spns2* in B cell trafficking that has to be tested in more detail in further experiments. Moreover, reconstitution of irradiated *Spns2*-ECKO mice with control bone marrow did not restore reduction of mature recirculating B cells in the bone marrow and peripheral blood (Supplemental Figure 18). These results demonstrate that S1P released by ECs through *Spns2* promotes the egress of immature B cells from the bone marrow into the blood.

Discussion

In the present study, we show for what we believe is the first time that *Spns2* expressed on ECs is essential for lymphocyte egress from the primary lymphoid organs. By analyzing the *Spns2*-deficient mice, we found that *Spns2* is an S1P transporter required for the egress of mature T cells and immature B cells from the thymus and the bone marrow, respectively, into the peripheral blood. In addition, by deleting *Spns2* in ECs and performing bone marrow reconstitution studies, we showed that *Spns2* regulates S1P secretion in ECs, but not in blood cells, to promote lymphocyte egress from primary lymphoid organs. Therefore, the

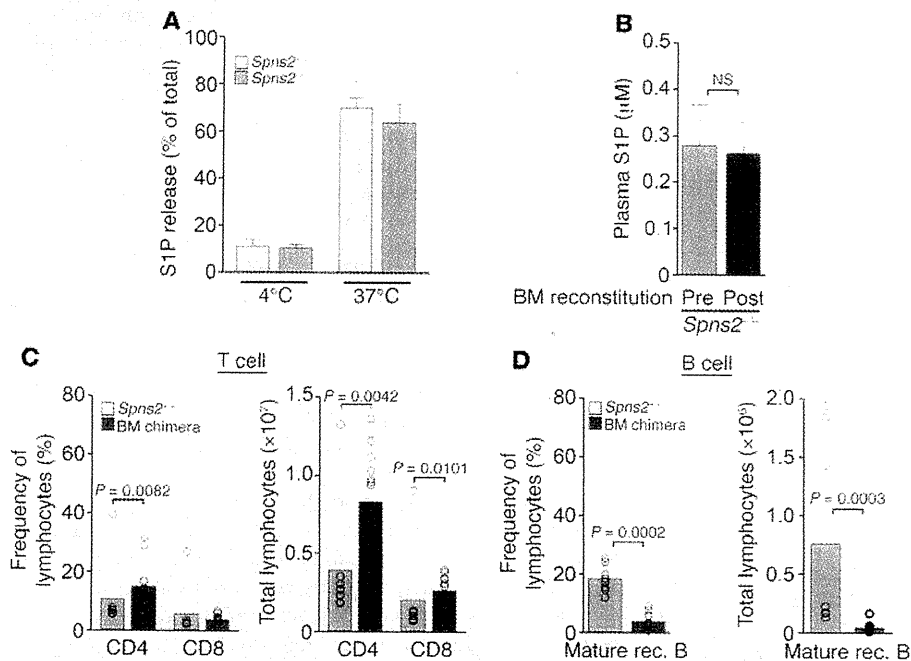


Figure 5

Spns2 is not involved in S1P release from blood cells. (A) Release of S1P by the blood cells isolated from control (*Spns2*^{+/+}) and *Spns2*^{-/-} mice. Cells were incubated at either 4°C or at 37°C for 90 minutes as indicated at the bottom. Data are expressed as a percentage of the total amount of S1P in the cells without incubation and shown as mean ± SD (n = 4). (B–D) *Spns2*^{-/-} mice were lethally irradiated and reconstituted with bone marrow from littermate control mice. (B) Plasma S1P concentrations of either *Spns2*^{-/-} mice (Pre) or of those reconstituted with WT bone marrow (Post) (n = 13). (C and D) Flow cytometric analyses of control (*Spns2*^{+/+}) and *Spns2*^{-/-} mice reconstituted with littermate control bone marrow (BM chimera). (C) Frequencies (left) and total numbers (right) of CD4 SP (CD4) and CD8 SP (CD8) T cells in the thymus are shown (*Spns2*^{+/+}, n = 8; BM chimera, n = 13). (D) Frequencies (left) and total numbers of mature recirculating B cells (CD19⁺IgM⁺IgD⁺) in the bone marrow are shown (*Spns2*^{+/+}, n = 8; BM chimera, n = 13).

present study on *Spns2* largely contributes to the understanding of S1P signaling, which is used in the egress of lymphocytes from primary lymphoid organs (1, 2, 4, 5).

Spns2 is the first S1P transporter functioning in mammals. Intracellularly generated S1P has to be transported out of the cell to stimulate its cell-surface receptors. Several lines of evidence obtained from in vitro studies have suggested the involvement of the ABC family of transporters in S1P release from several types of cells (22, 24, 29–32). However, their biological significance in vivo has remained unclear. In this study, we demonstrate *Spns2* as a key S1P transporter that regulates lymphocyte trafficking in mammals. Although *Spns2* regulates lymphocyte trafficking by inducing the release of S1P from ECs, this transporter may also function in other cells, since symblepharon was observed in *Spns2*^{-/-} mice, but not in *Spns2*-ECKO mice. On the other hand, *Spns2* appears not to be the only transporter of S1P in mammals because plasma S1P levels were partially but not completely decreased in *Spns2*^{-/-} mice compared with control mice. Although blood cells, especially erythrocytes, are thought to be the major cellular source of S1P in plasma (9, 23, 27), blood cells from *Spns2*^{-/-} mice still retained the ability to release S1P (Figure 5A). Thus, S1P release from blood cells appears to be mediated by S1P transporters other than *Spns2*. In addition, S1P transporters other than *Spns2* might also be involved in the release of S1P required for vascular development, since *Spns2*^{-/-} mice did

not show the defects in vascular development that can be observed in *S1p1*-deficient mice (48).

This study clearly reveals that *Spns2*-dependent S1P release from ECs is important for egress of mature T cells from the thymus into the peripheral blood. Thymic egress is strictly controlled by the S1P/S1P1 signaling pathway (1, 2, 4, 5). In the thymus, thymocytes differentiate into mature T cells, and subsequently express S1P1 through upregulation of Krüppel-like factor 2 (5, 49). S1P1-expressing mature T cells acquire responsiveness to S1P, thereby exiting from the thymus into the peripheral blood. Until recently, it has been assumed that the S1P gradient between the thymus and the blood is required for egress of mature T cells. However, recent evidence has suggested that plasma S1P is insufficient to promote thymic egress (9, 19). Importantly, egress of mature T cells from the thymus was impaired in *Spns2*^{-/-} mice even though the plasma contains enough concentration of S1P to stimulate lymphocyte S1P1 in vitro (10). Similarly, Zachariah and Cyster have recently reported that neural crest-derived pericytes covering the ECs release S1P responsible for thymic egress without influencing plasma S1P concentration (19). Therefore, mature T cells might be recruited to the abluminal

side of blood vessels by S1P locally released from both ECs and pericytes, and possibly exit into the peripheral blood in response to high concentrations of plasma S1P. However, further studies are needed to confirm this hypothesis.

Spns2 expressed on ECs of the blood vessels is also essential for B cell egress from the bone marrow. Although recent reports reveal the role of S1P/S1P1 signaling in the egress of immature B cells from the bone marrow (15, 16), a cellular source of S1P involved in this process has not been identified. In *Spns2*^{-/-} mice, the number of mature recirculating B cells was significantly decreased not only in the bone marrow but also in the blood, spleen, and peripheral lymph nodes, indicating a block in the egress of immature B cells from the bone marrow. Importantly, reconstitution of irradiated *Spns2*^{-/-} mice with WT bone marrow did not rescue the deficiency of mature recirculating B cells in the bone marrow. Furthermore, *Spns2*-ECKO mice also exhibited reduced numbers of mature recirculating B cells in the bone marrow, peripheral blood, spleen, and peripheral lymph nodes, as observed in *Spns2*^{-/-} mice. This phenotype was not rescued by reconstitution with control bone marrow. Thus, these results reveal for what we believe is the first time that ECs are the major cellular source of S1P necessary for the egress of immature B cells from the bone marrow. In the late stage of B cell development in the bone marrow, newly generated immature B cells placed in the parenchyma are first recruited into the sinusoidal compartment and subsequently

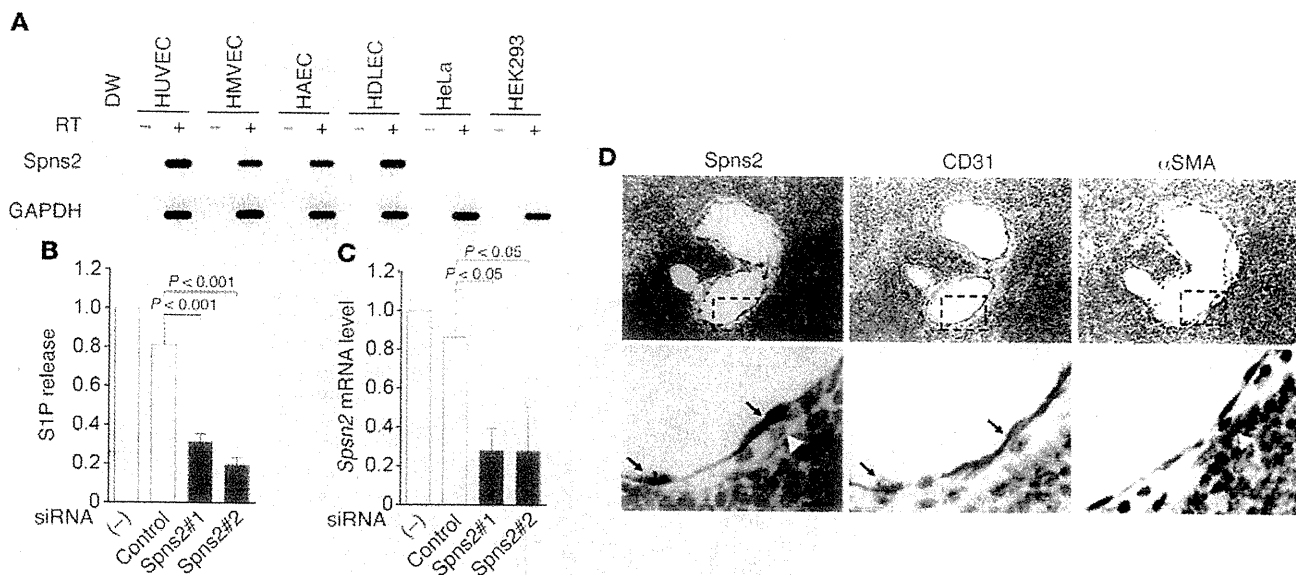


Figure 6

Spns2 is involved in S1P release from ECs. (A) Expression of Spns2 in ECs. RT-PCR analysis was performed to examine the expression of Spns2 in HUVECs, HMVECs, HAECs, HDLECs, HeLa, and HEK293 cells as indicated at the top. PCR was performed using specific primers for either Spns2 (upper panel) or GAPDH (lower panel). To verify the absence of contaminating genomic DNA, RT-PCR was also performed in the absence of reverse transcriptase (-). (B and C) S1P release from Spns2-depleted ECs. (B) Release of S1P by ECs transfected without (-) or with either control siRNA (control) or 2 independent siRNAs targeting Spns2 (Spns2#1 and Spns2#2). (C) Real-time RT-PCR analysis to assess the efficiency of siRNA-mediated Spns2 knockdown. In B and C, data are expressed relative to those observed in the untransfected cells and shown as mean \pm SD of 3 independent experiments. (D) In situ hybridization for Spns2 mRNA in thymus. Antisense probe was hybridized to thymus section (Spns2: purple). Serial sections were also stained with anti-CD31 (CD31: brown) and anti- α -SMA (brown) antibodies to identify ECs and pericytes, respectively. The boxed areas of upper panels are enlarged in lower panels. Arrows and white arrowheads indicate ECs and pericytes, respectively. Scale bars: 50 μ m (upper panels); 10 μ m (lower panels).

exported into the peripheral blood (50–52). Sinusoidal entry of immature B cells is thought to be a key step in bone marrow egress. Recently, it has been reported that S1P/S1P1 signaling promotes the movement of immature B cells from parenchyma to sinusoid, thereby facilitating egress of immature B cells from bone marrow (15, 16). Thus, bone marrow sinusoidal ECs may attract immature B cells from the parenchyma by producing S1P through Spns2 and thereby promoting the immature B cell egress into the peripheral blood.

The lymphocyte egress from secondary lymphoid organs such as lymph nodes and spleen also depends on S1P/S1P1 signaling. Pham et al. have recently reported that lymphatic ECs are an in vivo source of S1P required for lymphocyte egress from lymph nodes and Peyer patches (20). Since Spns2 is expressed not only in vascular ECs but also in lymphatic ECs, Spns2 may also regulate lymphocyte egress from lymph nodes by inducing the release of S1P from lymphatic ECs. However, to address this hypothesis, we need to analyze mice lacking Spns2 specifically in the lymphatic ECs because lymphocyte egress from primary lymphoid organs is severely impaired in global Spns2^{-/-} mice. It also remains elusive whether Spns2 is involved in lymphocyte egress from spleen. Thus, this will be a subject for future studies.

In conclusion, we demonstrate that Spns2 is a key S1P transporter involved in lymphocyte trafficking and further indicate that vascular ECs are the major source of S1P in vivo responsible for lymphocyte egress from the thymus and the bone marrow. Thus, this study not only reveals the crucial role of Spns2 as an S1P transporter in mammals, but also contributes to our understanding of molecular mechanisms of S1P-mediated lymphocyte trafficking.

Since S1P signaling is profoundly involved in the inflammatory and autoimmune diseases, such as multiple sclerosis, psoriasis, asthma, and rheumatoid arthritis, as well as in transplantation, Spns2 can be a potential therapeutic target for these diseases.

Methods

Generation of Spns2^{fl/fl} mice. Spns2^{fl/fl} mice (acc. no. CDB0705K; <http://www.cdb.riken.jp/arg/mutant%20mice%20list.html>), in which exon 2 is flanked by 2 loxP sites, were generated (Supplemental Figure 1A). TT2 ES cells derived from an F1 hybrid of C57BL/6 and CBA mice (53) were transfected with the targeting vector, selected in the presence of G418, and screened for homologous recombination by PCR and Southern blotting. Two ES clones were introduced into host embryos to generate chimeric mice. Chimeric mice with a high ES cell contribution were bred with the CMV-Cre mice (C57BL/6 strain background) expressing Cre recombinase under the control of cytomegalovirus promoter to generate heterozygous Spns2^{+/-} mice (Supplemental Figure 1). Spns2^{+/-} mice were intercrossed to obtain Spns2^{-/-} mice (75% C57BL/6 and 25% CBA genetic background). The chimeric mice were also crossed with the CMV-Flp mice (C57BL/6 strain background) expressing Flp recombinase under the control of cytomegalovirus early enhancer/chicken β -actin promoter to remove the PKG-Neo-pA cassette, resulting in Spns2 floxed mice (Supplemental Figure 1). To inactivate the Spns2 gene in ECs, the Spns2 floxed mice were bred with Tie2-Cre mice (C57BL/6 strain background), which carry the Cre recombinase driven by the Tie2 promoter (45, 46) and were provided by T.N. Sato (Nara Institute of Science and Technology, Nara, Japan) and M. Yanagisawa (University of Texas Southwestern Medical Center, Dallas, Texas, USA) (Supplemental Figure 1). For confirmation of cor-

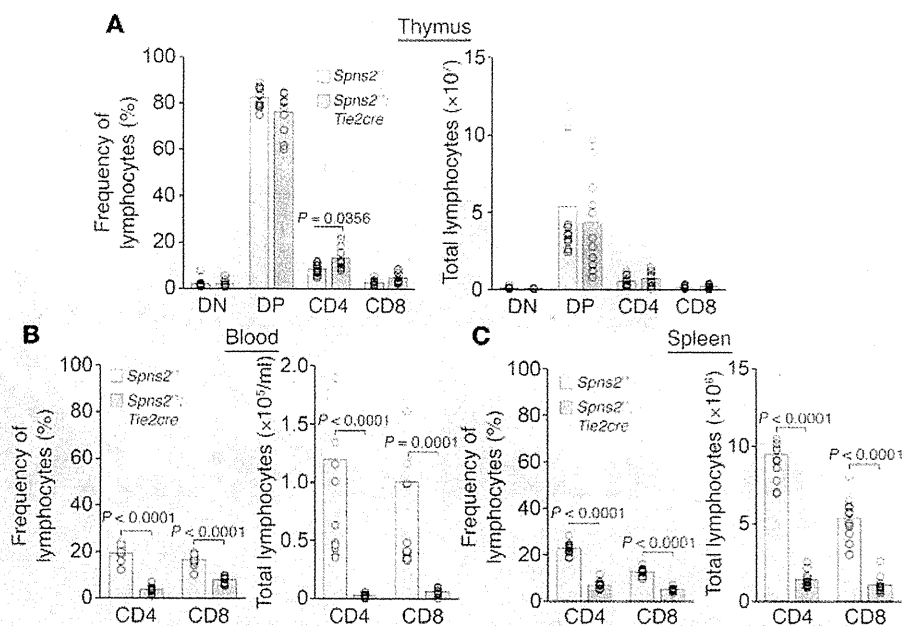


Figure 7

Spns2 expressed in ECs is required for mature T cell egress from thymus. (A–C) Flow cytometric analyses of lymphocytes of control (*Spns2^{+/+}*) or Spns2-ECKO (*Spns2^{-/-};Tie2Cre*) mice. (A) Frequencies (left) and numbers (right) of CD4/CD8 DN (DN), CD4/CD8 DP (DP), CD4 SP (CD4), and CD8 SP (CD8) thymocytes and T cells in thymus are shown ($n = 11$). (B) Frequencies and numbers of CD4 SP (CD4) and CD8 SP (CD8) T cells in peripheral lymph nodes are shown ($n = 11$). (C) Frequencies and numbers of CD4 SP (CD4) and CD8 SP (CD8) T cells in spleens are shown ($n = 11$). In A–C, bars and circles indicate averages and values for individual mice, respectively.

rect targeting, Southern blot analysis was performed with the probe located outside of the regions used in the targeting vector (Supplemental Figure 1). For the genotyping of mice, PCR was performed using a forward primer, 5'-AGGCTCATTTTCATGGCTGAT-3', and a reverse primer, 5'-AGCCCTGTGCTCTCTGTTGT-3', producing products of 552-bp fragment for WT allele, 842-bp fragment for floxed allele, and 316-bp fragment for deleted allele. All mice were housed under specific pathogen-free conditions.

RT-PCR and real-time RT-PCR. To check the expression of *Spns2* mRNA in *Spns2^{-/-}* mice, total RNA was extracted from the lungs using TRIzol reagent (Invitrogen) and reverse transcribed by random hexamer primers using Superscript II (Invitrogen) according to the manufacturer's instructions. PCR amplification was carried out with the following primer sets: PCR1, 5'-AAGAGGTGCAGACGTTGTCC-3' and 5'-CCACAGCTGAGGATCACCTT-3', for exons 1–3 of the mouse *Spns2*; and PCR2, 5'-ATGATGTGCCTGGAATGC-3' and 5'-TCAGACTTTCACGGATGCAG-3', for complete coding sequence of mouse *Spns2*.

To determine the expression of Spns2 in ECs, RT-PCR was performed using the gene-specific primers for human *SPNS2* (5'-ACTTTGGGGTCAAGGACCGA-3' and 5'-AATCACCTTCTGTTGAAGCG-3'). Amplification of *GAPDH* was also performed using the gene-specific primers for human *GAPDH* (5'-ATGGGGAAGGTGAAGGTCG-3' and 5'-GGGGT-CATTGATGGCAACAATA-3') in parallel as a control.

To assess the efficiency of siRNA-mediated knockdown of Spns2, total RNA was extracted from HUVECs transfected without or with either control siRNA or 2 independent siRNAs targeting Spns2 and subjected to quantitative real-time RT-PCR analysis using the QuantiFast SYBR Green RT-PCR Kit (QIAGEN) as described (54). For each reaction, 100 ng of total RNA was transcribed for 10 minutes at 50 °C, followed by a denaturation step at 95 °C for 5 minutes, 40 cycles of 10 seconds at 95 °C, and 30 seconds at 60 °C. Fluorescence data were collected and analyzed using Mastercycler ep realplex (Eppendorf). For normalization, expression of human *GAPDH* was determined in parallel as an endogenous control. The gene-specific primers used to amplify human *SPNS2* and *GAPDH* were the same as described above.

Cell culture, transfection, and siRNA-mediated gene silencing. HUVECs, human microvascular ECs (HMVECs), and human aortic ECs (HAECs) were purchased from Kurabo and maintained as described previously (55). Human

dermal lymphatic ECs (HDLECs) were obtained from Lonza and maintained in EC growth medium EGM-2 (Lonza). HeLa and HEK293 cells were cultured in DMEM (Nissui) supplemented with 10% fetal bovine serum and antibiotics (100 µg of streptomycin/ml and 100 U of penicillin/ml).

Stealth siRNAs targeted to human Spns2 (HSS151335 and HSS151336) were purchased from Invitrogen. As a control, siRNA duplexes with irrelevant sequences were used. HUVECs were transfected with 20 nM siRNA duplexes using Lipofectamine RNAi MAX reagent (Invitrogen). After incubation for 48 hours, the cells were used for the experiments.

Detection of subcellular localization of GFP-tagged Spns2. cDNAs encoding WT and mutant Spns2 were amplified using cDNAs derived from the lungs of WT and *Spns2^{-/-}* mice by RT-PCR, and cloned into pEGFP-N1 vector to construct the expression plasmids encoding WT and mutant Spns2 with a C-terminal GFP tag, respectively. HUVECs were transfected with the plasmid encoding either WT or mutant Spns2-GFP or with myristoylated GFP-encoding plasmid. GFP and phase contrast images were obtained using an IX81 inverted microscope (Olympus) equipped with a pE-1 LED excitation system (CoolLED).

S1P release from cultured cells. HEK293 cells were plated in 24-well plates (5×10^4 cells/well), cultured for 24 hours, and transfected with the expression plasmids indicated in the legend of Supplemental Figure 2D using Lipofectamine 2000 reagent (Invitrogen). After incubation for 24 hours, cells were incubated in 250 µl of serum-free DMEM containing 0.5 % fatty acid-free bovine serum albumin, 10 mM sodium glycerophosphate, 5 mM sodium fluoride, and 1 mM semicarbazide for 24 hours. To determine the role of Spns2 in S1P release from ECs, HUVECs transfected without or with either control siRNA or 2 independent Spns2 siRNAs were detached, replated in collagen-coated 24-well plates (2.5×10^5 cells/well), and cultured for 12 hours. The cells were then washed twice with Medium 199 (Invitrogen) and incubated in 200 µl of Medium 199 containing 20 mM HEPES, pH 7.4, 10 mM sodium glycerophosphate, 5 mM sodium fluoride, 1 mM semicarbazide, 0.5% fatty acid free bovine serum albumin, 40 ng/ml vascular endothelial growth factor, 40 ng/ml fibroblast growth factor-2, and 400 ng/ml angiotensin-1 for 12 hours. After incubation, conditioned medium was collected and centrifuged at 15,000 g for 5 minutes at 4 °C to remove cell debris. S1P levels in the conditioned medium were determined as described below.

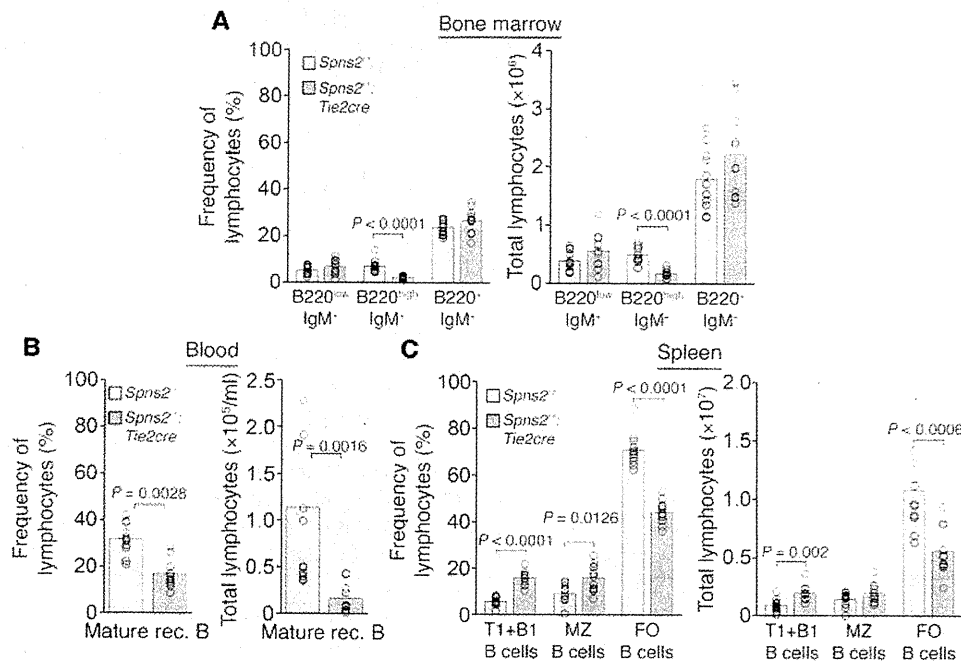


Figure 8

Spns2 expressed in ECs is required for immature B cell egress from bone marrow. (A–C) Flow cytometric analyses of lymphocytes of control (*Spns2^{fl/fl}*) or *Spns2*-ECKO (*Spns2^{fl/fl};Tie2Cre*) mice. (A) Frequencies (left) and numbers (right) of pro-/pre-B cells (B220⁺IgM⁻), immature B cells (B220^{hi}IgM⁺), and mature recirculating B cells (B220^{hi}IgM⁺) in bone marrow are shown (*n* = 11). (B) Frequencies (left) and numbers (right) of mature recirculating B (Mature rec. B) cells (CD19⁺CD23⁺IgD⁺) in peripheral blood are shown (*n* = 11). (C) Frequencies (left) and numbers (right) of T1 and B1 B cells (T1+B1), MZ, and follicular B cells in spleens are shown (*n* = 11). T1 and B1 B cells, MZ B cells, and follicular B cells were phenotypically defined as described in the legend of Figure 3D. In A–C, bars and circles indicate averages and values for individual mice, respectively.

Quantification of S1P using LC-MS/MS. Quantification of S1P was performed according to previously described methods (56) with minor modifications. Briefly, plasma and conditioned medium were mixed and sonicated with 10-fold volume of methanol and an internal standard (C17-S1P). Similarly, S1P extraction from cells was performed by homogenizing and sonicating cells in methanol. After centrifugation at 21,500 g, the resulting supernatant was recovered and used for the LC-MS/MS analysis. Then 20 μ l of methanol extract was injected and separated by Nanospace LC (Shiseido) equipped with a C18 CAPCELL PAK ACR column (1.5 \times 250 mm; Shiseido), using a gradient of solvent A (5 mM ammonium formate in water) and solvent B (5 mM ammonium formate in 95% [v/v] acetonitrile). Elution was sequentially ionized with an ESI probe, and the parent ion (*m/z* 380.2) and the fragment ion (*m/z* 264.2) were monitored in the positive mode by a Quantum Ultra Triple Quadrupole Mass Spectrometer (Thermo Fisher Scientific). Similarly, other lysophospholipids, including lysophosphatidic acid (LPA), lysophosphatidylcholine (LPC), lysophosphatidylethanolamine (LPE), lysophosphatidylglycerol (LPG), lysophosphatidylinositol (LPI), and lysophosphatidylserine (LPS), were extracted with methanol and analyzed by the LC-MS/MS system. For each lysophospholipid class, 12 acyl chains (14:0, 16:0, 16:1, 18:0, 18:1, 18:2, 18:3, 20:3, 20:4, 20:5, 22:5, and 22:6) were monitored.

For quantification of HDL- and albumin-bound S1P, mouse plasma was subjected to size-exclusion chromatography according to previously described methods (57) with some modifications. Briefly, 100 μ l of plasma was loaded onto a Superose 12 column (GE Healthcare) using an ÄKTA Explorer System (GE Healthcare) and eluted with PBS at 0.25 ml/min at

4°C. Fractions were collected every 2 minutes (0.5 ml). S1P concentration in each fraction was determined by LC-MS/MS as described above.

Biochemical and hematological test of blood. Blood was collected from WT (*Spns2^{fl/fl}*, *n* = 4) and *Spns2^{-/-}* (*Spns2^{-/-}*, *n* = 4) mice via the abdominal aorta under inhalation anesthesia (isoflurane) using EDTA as an anticoagulant. Blood biochemistry parameters (total protein, total bilirubin, aspartate aminotransferase, alanine aminotransferase, triglycerol, glucose, blood urea nitrogen, and albumin) were determined by using a blood biochemical analyzer, Fuji DRI-CHEM 3500V (Fuji Film). Hematology and blood clotting parameters (white blood cells, red blood cells, platelets, hemoglobin, hematocrit, mean corpuscular volume, mean corpuscular hemoglobin, and mean corpuscular hemoglobin concentration) were determined by using an XT-1800iv hematology analyzer (Sysmex).

Antibodies and flow cytometric analysis. Unless otherwise stated, all anti-mouse monoclonal antibodies were obtained from eBiosciences Inc. Antibodies used for cell-surface staining were PE-conjugated anti-CD19 (ebio1D3), anti-CD8 (53-6.7), and anti-CD23 (B3B4); FITC-conjugated anti-B220 (RA3-6B2), anti-CD19

(1D3) (BD Biosciences), anti-CD8 (53-6.7) and anti-CD69 (H1.2F3) (BD Biosciences); APC-conjugated anti-CD62L (MEL-14) (BioLegend); Pacific Blue-conjugated anti-IgD (11-26) and anti-CD4 (RM4-5) (BD Biosciences); PeCy7-conjugated anti-IgM (II/41); and PerCP-Cy5.5 conjugated anti-CD21/CD35 (7E9) (BioLegend). Single-cell suspensions of freshly isolated thymus, spleen, peripheral lymph nodes (inguinal, axillary, and brachial), and total bone marrow cells of femur and tibia were subsequently incubated with anti-CD16/CD32 for 10 minutes, followed by staining with a combination of conjugated antibodies in FACS buffer (PBS + 4% heat-inactivated FCS + 2 mM EDTA) for 30 minutes. Before antibody staining, 250 μ l of freshly isolated blood was treated with heparin solution, and red blood cells were lysed with BD Pharm Lyse solution (BD Biosciences) according to the manufacturer's protocol. Stained cells were analyzed on a FACS-Canto II Flow Cytometer (BD Biosciences) equipped with blue (488 nm), violet (405 nm), and red (633 nm) lasers. FACS data were statistically analyzed with FlowJo software (TreeStar Inc.).

Histopathology and immunohistochemistry. Tissue samples from the spleen, thymus, axillary lymph nodes, mesenteric lymph nodes, and intestine (including Peyer patches) were collected from WT (*Spns2^{fl/fl}*, *n* = 3) and *Spns2^{-/-}* (*Spns2^{-/-}*, *n* = 3) mice and fixed in 20% neutral phosphate-buffered formalin. Each paraffin-embedded tissue was cut into 4- μ m thickness and stained with H&E for light microscopy.

For immunohistochemistry, paraffin was then removed from the sections and antigen retrieval was performed in 10 mM citrate buffer (pH 6.0) by placing the sections in a pressure cooker for 3 minutes. Endogenous